Article

A receptor–channel trio conducts Ca^{2+} signalling for pollen tube reception

https://doi.org/10.1038/s41586-022-04923-7

Received: 23 July 2021

Accepted: 31 May 2022

Published online: 6 July 2022

Check for updates

Qifei Gao[1], Chao Wang[1], Yasheng Xi[1], Qiaolin Shao[1], Legong Li[2] & Sheng Luan[1]✉

Precise signalling between pollen tubes and synergid cells in the ovule initiates fertilization in flowering plants[1]. Contact of the pollen tube with the ovule triggers calcium spiking in the synergids[2,3] that induces pollen tube rupture and sperm release. This process, termed pollen tube reception, entails the action of three synergid-expressed proteins in *Arabidopsis*: FERONIA (FER), a receptor-like kinase; LORELEI (LRE), a glycosylphosphatidylinositol-anchored protein; and NORTIA (NTA), a transmembrane protein of unknown function[4–6]. Genetic analyses have placed these three proteins in the same pathway; however, it remains unknown how they work together to enable synergid–pollen tube communication. Here we identify two pollen-tube-derived small peptides[7] that belong to the rapid alkalinization factor (RALF) family[8] as ligands for the FER–LRE co-receptor, which in turn recruits NTA to the plasma membrane. NTA functions as a calmodulin-gated calcium channel required for calcium spiking in the synergid. We also reconstitute the biochemical pathway in which FER–LRE perceives pollen-tube-derived peptides to activate the NTA calcium channel and initiate calcium spiking, a second messenger for pollen tube reception. The FER–LRE–NTA trio therefore forms a previously unanticipated receptor–channel complex in the female cell to recognize male signals and trigger the fertilization process.

As a ubiquitous second messenger, Ca^{2+} regulates many aspects of physiology and development in both animals and plants[9–11], including reproduction. In animals, Ca^{2+} signals drive the motility of sperm[12] and forecast successful fertilization[13]. In flowering plants, sperm are immobile and require a special delivery structure called the pollen tube, which navigates the female tissue and finds the ovule before releasing sperm[1]. From pollen germination to pollen tube guidance and pollen tube reception, each step requires intricate Ca^{2+} signalling[14]. However, the molecular mechanism underlying Ca^{2+} signalling in plant reproduction remains largely unknown. During pollen tube reception, interactions between the pollen tube and synergids in the ovule activates Ca^{2+} oscillations in both partners, which leads to the rupture of the pollen tube and synergid cell death and the initiation of fertilization[2,3,15,16]. On the female side, FER, LRE and NTA are three components from the same pathway required for synergid Ca^{2+} spiking in response to pollen tube arrival, but little is known regarding how they work together to mediate Ca^{2+} entry. We show here that pollen tube RALFs bind to FER–LRE co-receptors, which recruit NTA, a calcium channel, to form a receptor–channel assembly. This tri-molecular complex is regulated by Ca^{2+}/calmodulin (CaM)-dependent feedback inhibition to drive Ca^{2+} oscillations in the synergid.

RALFs trigger synergid Ca^{2+} oscillation

FER and LRE are both required for pollen tube reception and may function as a co-receptor for unknown signals derived from pollen tubes[4,5,17–20]. We hypothesized that such signals may be mediated by RALF family peptides because some RALFs bind to either FER alone[21,22] or to both FER and LRE-like proteins (LLGs) in other processes[23–25]. Among the 37 *Arabidopsis* RALFs, at least 8 (RALF4, RALF8, RALF9, RALF15, RALF19, RALF25, RALF26 and RALF30) are expressed in pollen tubes[7]. We expressed and purified the eight pollen-tube-derived RALF peptides and examined their interaction with FER[23]. We also included an ovule-derived RALF peptide (RALF34) that is closely related to pollen tube RALFs such as RALF4 and RALF19. The extracellular domain of FER (FER_{ex}) pulled down RALF4, RALF19 and RALF34 (Fig. 1a and Supplementary Fig. 1a). Consistent with this result, RALF4 and RALF19 acted antagonistically with RALF34 for pollen tube integrity through interactions with the same receptors of the FER family[7].

As ligands for FER–LLG co-receptors, RALFs enhance interactions between FER and LLGs[23]. Consistent with this model, RALF4, RALF19 and RALF34 enhanced the interaction between GST-tagged LRE and MBP-tagged FER_{ex}, whereas several other RALFs did not (Fig. 1b, bottom, and Supplementary Fig. 1b). This observation was confirmed by co-immunoprecipitation (co-IP) assays with total protein samples from *Nicotiana benthamiana* leaf tissue expressing LRE–Myc and FERK565R–Flag (Fig. 1c and Supplementary Fig. 1c). RALF4 is secreted into the apoplast of the pollen tube[26], and our promoter–β-glucuronidase (GUS) analysis confirmed the expression of RALF4 and RALF19 during pollen tube reception (Extended Data Fig. 1a). This result suggests that RALF4 and RALF19 interact with FER and LRE in the synergid. In summary, FER–LRE may function as co-receptors for pollen tube RALFs, including RALF4 and RALF19.

In response to pollen tube arrival, the synergids produce specific Ca^{2+} fluctuations required for pollen tube reception[2,3]. If RALFs signal the arrival of the pollen tube, they should produce a similar Ca^{2+} entry

[1]Department of Plant and Microbial Biology, University of California at Berkeley, Berkeley, CA, USA. [2]College of Life Sciences, Capital Normal University, Beijing, China. ✉e-mail: sluan@berkeley.edu

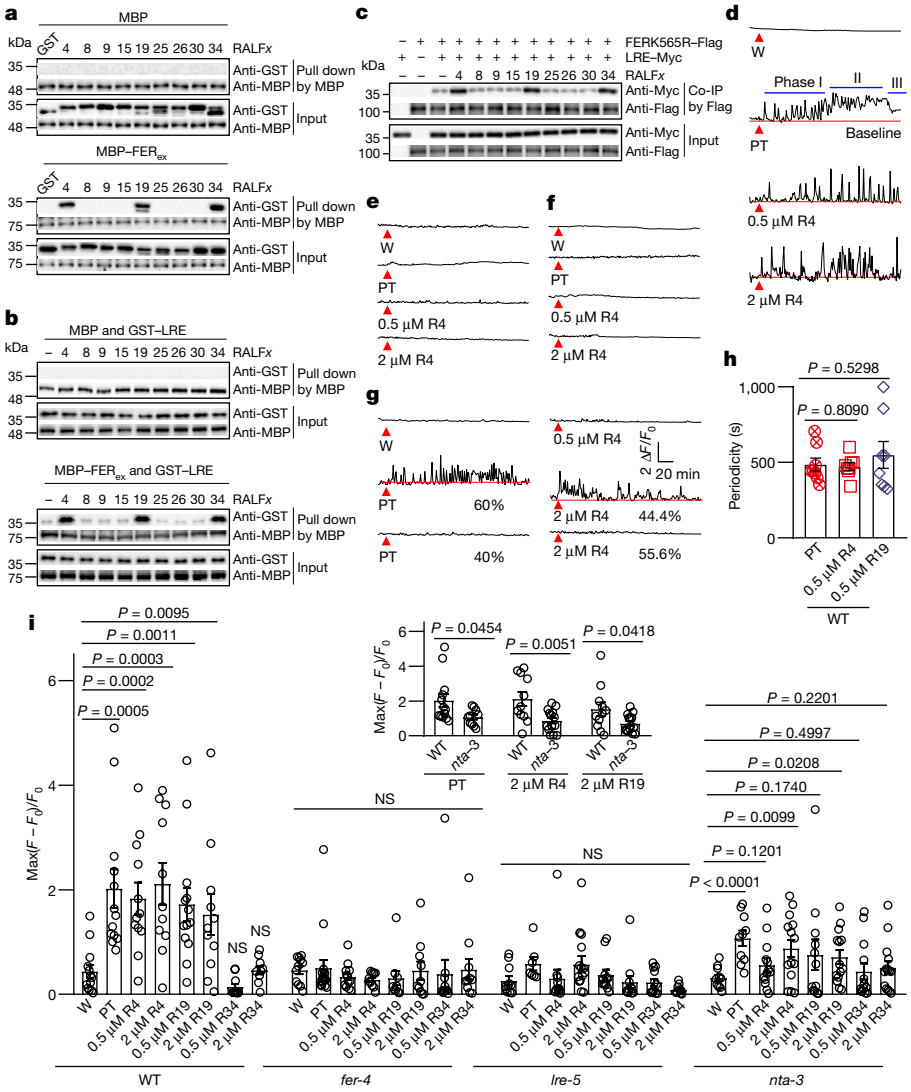

Fig. 1 | Pollen-derived RALFs bind to FER–LRE and trigger synergid $[Ca^{2+}]_{cyt}$ changes in a FER–LRE–NTA-dependent manner. a, Pull-down assays showing the interaction of GST-tagged RALFs and MBP-tagged ectodomains of FER (FER_{ex}). Amylose resin was used to pull down MBP, followed by western blotting with antibodies against GST and MBP. $n = 3$ independent repeats. **b**, Interaction of GST-tagged LRE and MBP-tagged ectodomains of FER with or without RALFs (RALF*x*; each 100 nM) as indicated. Amylose resin pull-down and western blotting was performed as in **a**. $n = 3$ independent repeats. **c**, Co-IP of Myc-tagged LRE and Flag-tagged FERK565R expressed in *N. benthamiana* leaves with or without the addition of RALFs (each 5 μM) as indicated. Anti-Flag M2 affinity beads were used in co-IP, and western blots were probed with antibodies against Myc and Flag. $n = 3$ independent repeats. **d**–**g**, Representative Ca^{2+} spiking patterns in synergids in response to pollen tube (PT) arrival or to 0.5 μM or 2 μM RALF4 (R4) for WT (**d**), *fer-4* (**e**), *lre-5* (**f**) and *nta-3* (**g**). W, water. **h**, Ca^{2+} oscillation periodicity of WT synergids in response to PT arrival or 0.5 μM RALF4 and RALF19 (R19). $n = 8$ ovules. **i**, The peak values of Ca^{2+} spiking as in **d**–**g**. *n* values are shown in Extended Data Fig. 3. Ovules were isolated from Col-0, *fer-4*, *lre-5* and *nta-3* flowers harbouring the synergid-specific GCaMP6, and fluorescence was recorded using an inverted microscope. Red triangles indicate time points at which the PT arrived or RALF4 was applied. Error bars depict the mean ± s.e.m. All *P* values were determined by two-tailed Student's *t*-test. NS, not significant.

pattern in the synergids when applied to isolated ovules in vitro. We generated transgenic plants that express the Ca^{2+} indicator GCaMP6s[27] driven by a synergid-specific promoter (p*MYB98*)[28] and examined changes in cytosolic calcium concentration ($[Ca^{2+}]_{cyt}$) in the synergids in response to RALFs. In the wild-type (WT) synergids, RALF4 and RALF19, but not RALF34, induced increases in $[Ca^{2+}]_{cyt}$ (Fig. 1d,i and Supplementary Videos 1, 2 and 3), which is consistent with the idea that RALF34 binds to the same receptors but functions differently[7]. Several other pollen tube RALFs (RALF8, RALF9, RALF15, RALF25, RALF26 and RALF30) that did not bind FER also failed to induce synergid $[Ca^{2+}]_{cyt}$ changes (Extended Data Fig. 2). In the pollen tube reception assay, the receptive synergid and nonreceptive synergid in one ovule showed distinct Ca^{2+} spikes[2]. However, exogenous RALF4 and RALF19 induced similar Ca^{2+} transients in both synergid cells in one ovule, which suggests that RALFs in the solution may have diffused evenly towards the two synergids. By contrast, the pollen tube positions itself closer to one of the two synergids, which leads to asymmetrical signalling.

We then compared synergid Ca^{2+} changes triggered by the pollen tube[2,3] with those induced by RALFs. As reported earlier[3], synergid Ca^{2+} dynamics proceeded in three phases as the pollen tube progressed to reception: (1) $[Ca^{2+}]_{cyt}$ oscillated at a regular pace when the pollen tube enters the micropyle and approaches the synergid; (2) $[Ca^{2+}]_{cyt}$ was sustained at a higher level after the pollen tube penetrates the synergid; (3) $[Ca^{2+}]_{cyt}$ was reduced when the synergid collapses. The amplitude and periodicity of Ca^{2+} oscillations triggered by RALF4 and RALF19 were similar to phase I of Ca^{2+} spiking induced by the pollen tube (Fig. 1d–i, Extended Data Fig. 3 and Supplementary Video 4). This result suggests

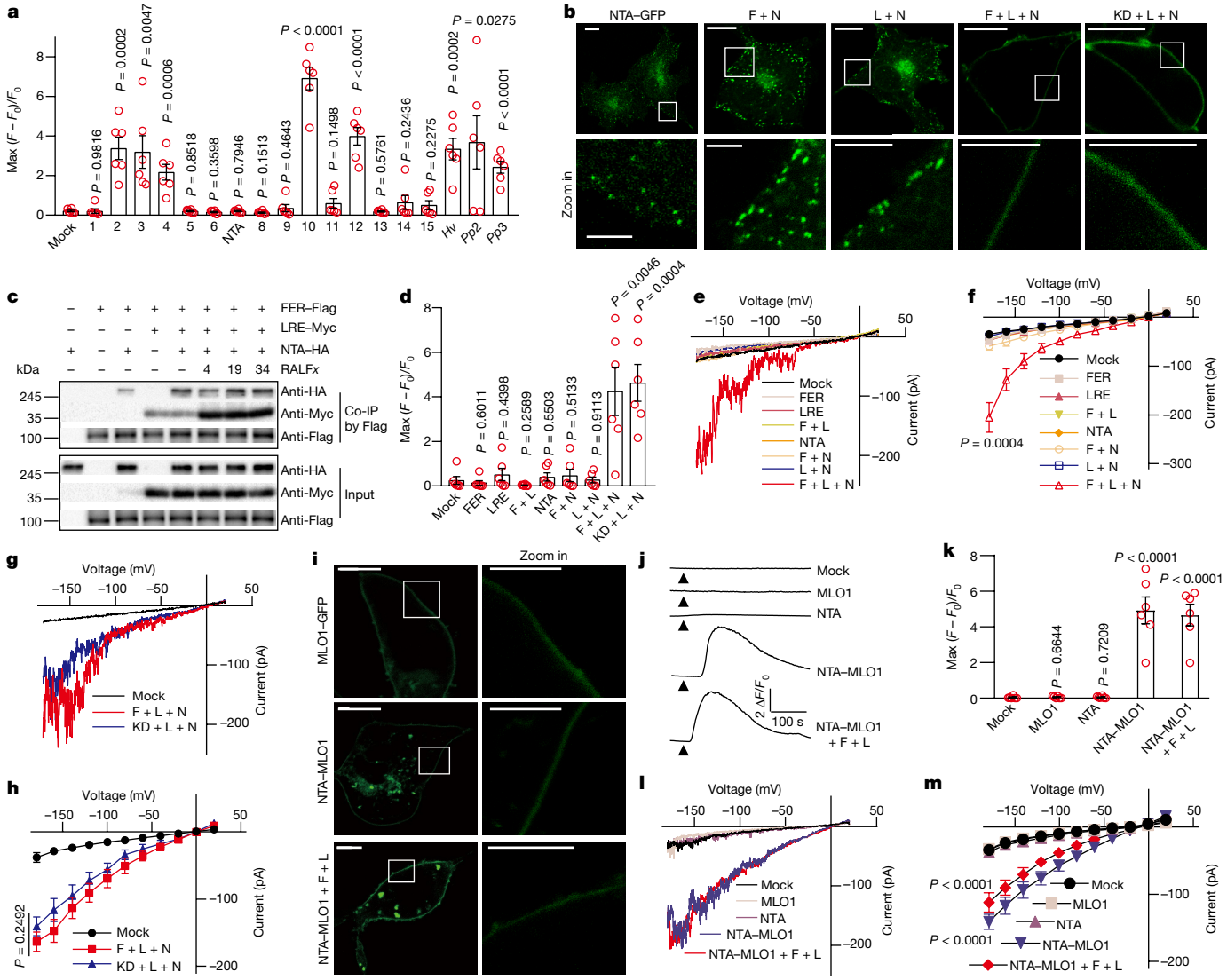

Fig. 2 | MLO family proteins, including NTA, are Ca^{2+}-permeable channels. **a**, $[Ca^{2+}]_{cyt}$ increases measured by single-cell fluorescence imaging in COS7 cells expressing various MLO proteins 1–15 (*At*MLO1–*At*MLO15). *Hv*, *Hv*MLO; *Pp*2, *Pp*MLO2; *Pp*3, *Pp*MLO3. **b**, FER and LRE facilitated the PM localization of NTA–GFP. The white rectangle indicates the area magnified in the bottom panels. $n = 3$ independent repeats. Scale bars, 5 µm (bottom row) or 10 µm (top row). **c**, Co-IP of HA-tagged NTA, Myc-tagged LRE and Flag-tagged FER expressed in *Xenopus* oocytes with or without the addition of RALFs (each 5 µM) as indicated. Anti-Flag M2 affinity beads were used to co-IP, and western blots were probed with antibodies against Myc, HA and Flag. $n = 3$ independent repeats. **d**, $[Ca^{2+}]_{cyt}$ increases measured by single-cell imaging of COS7 cells expressing NTA (N), FER (F), FERK565R (kinase-dead version) (KD) or LRE (L), or combinations thereof. **e**,**f**, Typical whole-cell recordings (**e**) and current–voltage curves (**f**) of inward currents in HEK293T cells expressing NTA, FER and LRE. **g**,**h**, Similar analyses were conducted for HEK293T cells expressing NTA, LRE and the kinase-dead version of FER. **i**, The C-terminal cytosolic tail of MLO1 facilitated the PM localization of NTA–GFP. NTA–MLO1 denotes the chimeric protein of NTA and MLO1 C-terminal tail. $n = 3$ independent repeats. Scale bars, 5 µm (right column) or 10 µm (left column). **j**,**k**, Representative cytosolic Ca^{2+} spiking curves (**j**) and statistical analysis of peak values (**k**) in COS7 cells expressing the NTA–MLO1 chimeric or original channels. **l**,**m**, Typical whole-cell recordings (**l**) and current–voltage curves (**m**) of inward currents in HEK293T cells expressing the NTA-MLO1 chimeric or original channels. For Ca^{2+} imaging in COS7 cells, $n = 6$ replicates, and about 60 cells were imaged in each duplicate. For patch-clamp, $n = 8$ cells. Error bars depict the mean ± s.e.m. All *P* values were determined by two-tailed Student's *t*-test.

that pollen-tube-derived RALF4 and RALF19 mimic the early phase of pollen tube arrival before mechanical penetration.

We then tested whether RALF4 and RALF19 induced such Ca^{2+} spiking in a FER–LRE-dependent manner. Synergids from *fer-4* and *lre-5* mutants failed to respond to RALF4, RALF19 or pollen tube arrival[3] (Fig. 1e,f,i, Extended Data Fig. 3 and Supplementary Videos 5 and 6). In addition to the *fer* and *lre* mutants, a mutant lacking NTA was non-responsive to 0.5 µM RALF4/19, although a portion of the *nta-3* synergid showed weaker responses to an increased level of RALF4/19 (2 µM) in Ca^{2+} imaging assays (Fig. 1g,i, Extended Data Fig. 3 and Supplementary Video 7). Compared to the *fer* and *lre* mutants, the weaker defect in *nta-3* suggests that there may be partial functional redundancy with another NTA-like component in this system.

MLO proteins are Ca^{2+} channels

The NTA protein is a member of the MILDEW RESISTANCE LOCUS O (MLO) protein family[6]. Originally discovered as a genetic determinant for resistance against powdery mildew in barley[29], the MLO proteins feature multi-transmembrane domains and a CaM-binding domain (CaMBD)[30,31]. The *Arabidopsis* genome encodes 15 MLO proteins (*At*MLO1–*At*MLO15), some of which are functionally linked to root thigmomorphogenesis[32], powdery mildew susceptibility[33] and pollen tube growth[34]. NTA (*At*MLO7) is specifically expressed in synergids and appears to function downstream of the FER–LRE module in pollen tube reception[6]. The biochemical function of MLO proteins remains unknown, which represents a crucial

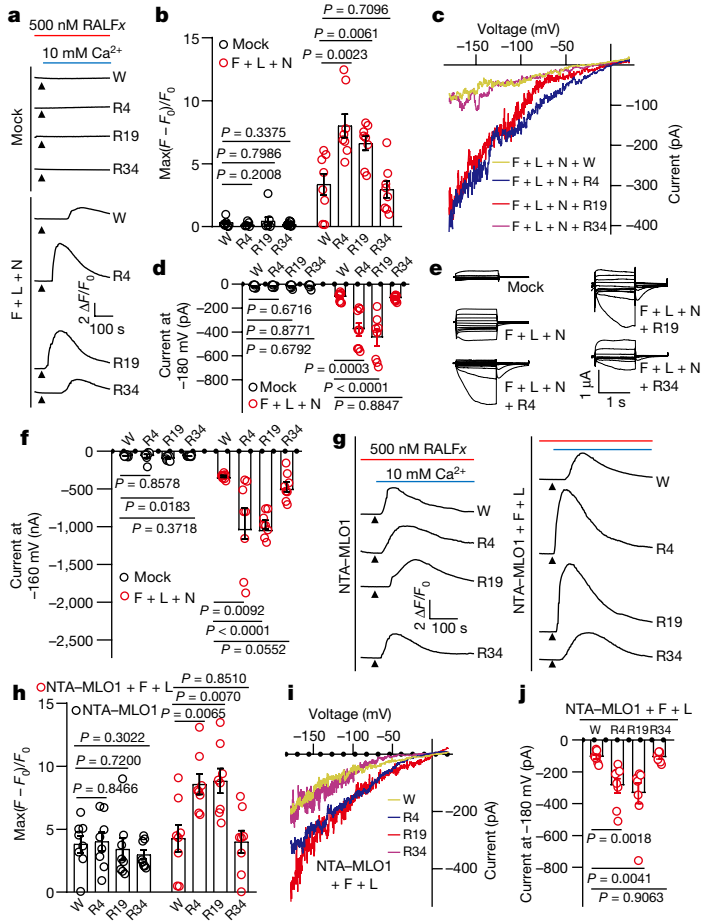

Fig. 3 | RALFs enhance the Ca^{2+} channel activity of the FER–LRE–NTA trio. **a**,**b**, Representative cytosolic Ca^{2+} spiking curves (**a**) and statistical analysis of peak values (**b**) in COS7 cells expressing the FER–LRE–NTA trio or mock cells treated with various RALFs. The arrowheads indicate the time points at which 10 mM Ca^{2+} was applied. **c**,**d**, Typical whole-cell recording traces using the ramping protocol (**c**) and amplitudes at −180 mV (**d**) of Ca^{2+}-permeable inward currents in HEK293T cells expressing FER–LRE–NTA or mock cells treated with various RALFs. **e**,**f**, Typical two-electrode voltage-clamp recordings (**e**) and current amplitudes at −160 mV (**f**) of inward currents in *Xenopus* oocytes expressing FER–LRE–NTA or mock water-injected oocytes treated with various RALFs. **g**,**h**, Representative cytosolic Ca^{2+} spiking curves (**g**) and statistical analysis of peak values (**h**) in COS7 cells expressing the chimeric NTA–MLO1 or FER–LRE–NTA–MLO1 treated with various RALFs. **i**,**j**, Typical whole-cell recording traces using the ramping protocol (**i**) and amplitudes at −180 mV (**j**) of Ca^{2+}-permeable inward currents in HEK293T cells expressing FER–LRE–NTA–MLO1 treated with various RALFs. For Ca^{2+} imaging in COS7 cells, $n = 8$ replicates, and about 60 cells were imaged in each duplicate. For HEK293T cell recordings, $n = 8$ cells. For oocyte recordings, $n = 8$ oocytes. Error bars depict the mean ± s.e.m. All P values were determined by two-tailed Student's t-test.

gap in knowledge with respect to the signalling pathways in which they participate[31]. Genetic analyses of NTA indicates that it works together with FER–LRE co-receptors in the same pathway to induce Ca^{2+} influx. Because NTA and other MLO proteins are multi-transmembrane proteins, we hypothesized that NTA is one of the missing Ca^{2+}-transporting proteins responsible for synergid Ca^{2+} entry.

To test whether MLO proteins transport Ca^{2+}, we performed Ca^{2+} transport assays with all 15 MLO members from *Arabidopsis* (*At*MLO1–*At*MLO15), the barley MLO (*Hv*MLO) and 2 MLO members from *Physcomitrella patens* (*Pp*MLO2 and *Pp*MLO3), which represent dicot, monocot and basal land plant MLO proteins, respectively. In single-cell Ca^{2+} imaging assays[35], *At*MLO2, *At*MLO3, *At*MLO4, *At*MLO10, *At*MLO12, *Hv*MLO, *Pp*MLO2 and *Pp*MLO3 mediated Ca^{2+} entry when expressed in COS7 cells (Fig. 2a and Extended Data Fig. 4). To confirm these Ca^{2+} imaging results, we used patch-clamping to directly measure the transport activity of *At*MLO2 expressed in HEK292T cells. We recorded large inward currents mediated by *At*MLO2 that depended on external Ca^{2+} concentrations (Extended Data Fig. 5a,b). Moreover, *At*MLO2 was permeable to Ba^{2+} and Mg^{2+}, but not to K^+ or Na^+ (Extended Data Fig. 5c–f,i–l). Furthermore, two typical Ca^{2+} channel blockers, lanthanum (La^{3+}) and gadolinium (Gd^{3+}), inhibited the *At*MLO2-mediated inward currents (Extended Data Fig. 5g,h). Similar to *At*MLO2, *Hv*MLO also mediated Ca^{2+} influx (Extended Data Fig. 6). These results indicate that MLO proteins function as Ca^{2+}-permeable channels.

The FER–LRE–NTA trio mediates Ca^{2+} entry

Many of the tested MLO proteins (including NTA) failed to mediate Ca^{2+} entry in HEK293T or COS7 cells (Fig. 2a, Extended Data Fig. 4 and Supplementary Videos 8 and 9). We speculated that they may require other components to be active or they may not be properly targeted to the plasma membrane (PM). Indeed, NTA primarily accumulates in a Golgi-associated compartment[36] and relocates to the synergid filiform apparatus in a FER- and LRE-dependent manner[6,37]. In our Ca^{2+} transport assays, PM localization would be crucial for mediating Ca^{2+} entry if NTA is indeed a Ca^{2+} channel. NTA–GFP was largely localized to intracellular punctate structures in COS7 cells (Fig. 2b). When co-expressed with FER and LRE, however, NTA–GFP was targeted to the PM (Fig. 2b). Such PM targeting was not achieved by co-expressing NTA–GFP with either FER or LRE alone, which is consistent with the finding that LRE–LLG1 physically interacts with and chaperones FER to the PM[19] and that FER is required for the redistribution of NTA to the PM[6]. We further showed that NTA directly interacted with FER and that LRE enhanced such an interaction (Fig. 2c and Supplementary Fig. 1d), which indicates that FER, LRE and NTA form a complex, which we refer here as the NTA trio.

As FER and LRE together target NTA to the PM, we tested whether the NTA trio produces a functional channel at the PM. We co-expressed NTA with FER and LRE in COS7 and HEK293T cells and then performed imaging assays and patch-clamp recordings, which showed that NTA mediated Ca^{2+} influx (Fig. 2d–f, Supplementary Video 10 and Extended Data Fig. 7). Similar to *At*MLO2 and *Hv*MLO, the NTA trio conducted currents carried by divalent cations (Ca^{2+}, Ba^{2+} and Mg^{2+}), but not monovalent cations (K^+ and Na^+) (Extended Data Fig. 8). The Ca^{2+} channel activity of the NTA trio was inhibited by La^{3+} and Gd^{3+}, which also blocked synergid Ca^{2+} spiking (Extended Data Fig. 8). The kinase-dead version of FER also formed an active NTA trio (Fig. 2d,g,h), which is consistent with an earlier finding that the kinase activity of FER is not required for pollen tube reception[38,39].

Our data suggest that NTA is an active Ca^{2+} channel but requires FER–LRE for targeting it to the PM. We tested this idea by constructing a PM-localized chimeric NTA–MLO1 protein[36,37], which showed that NTA–MLO1 mediated Ca^{2+} influx independently of FER–LRE (Fig. 2j–m).

RALFs enhance FER–LRE–NTA activity

We then tested the effect of RALFs on the activity of the NTA trio. RALF4 and RALF19, but not RALF34, significantly enhanced the Ca^{2+} channel activity of the NTA trio (Fig. 3a–d), which is consistent with the finding that RALF4 and RALF19 strongly induce increases in synergid Ca^{2+} (Fig. 1d,i). We further confirmed this observation by reconstituting the RALF–FER–LRE–NTA pathway in *Xenopus* oocytes and monitoring channel activity by two-electrode voltage-clamp assays (Fig. 3e,f). The chimeric NTA–MLO1 co-expressed with FER and LRE was also enhanced by RALF4 and RALF19, but not by RALF34 (Fig. 3g–j). Regarding the mechanism underlying the RALF4- and RALF19-dependent activation of the channel, a previous study[6] has shown that NTA is redistributed to the filiform apparatus of the synergid following the arrival of the pollen tube. We examined the PM localization of NTA in response to RALFs, but did not observe any discernible effect of RALF4 and RALF19

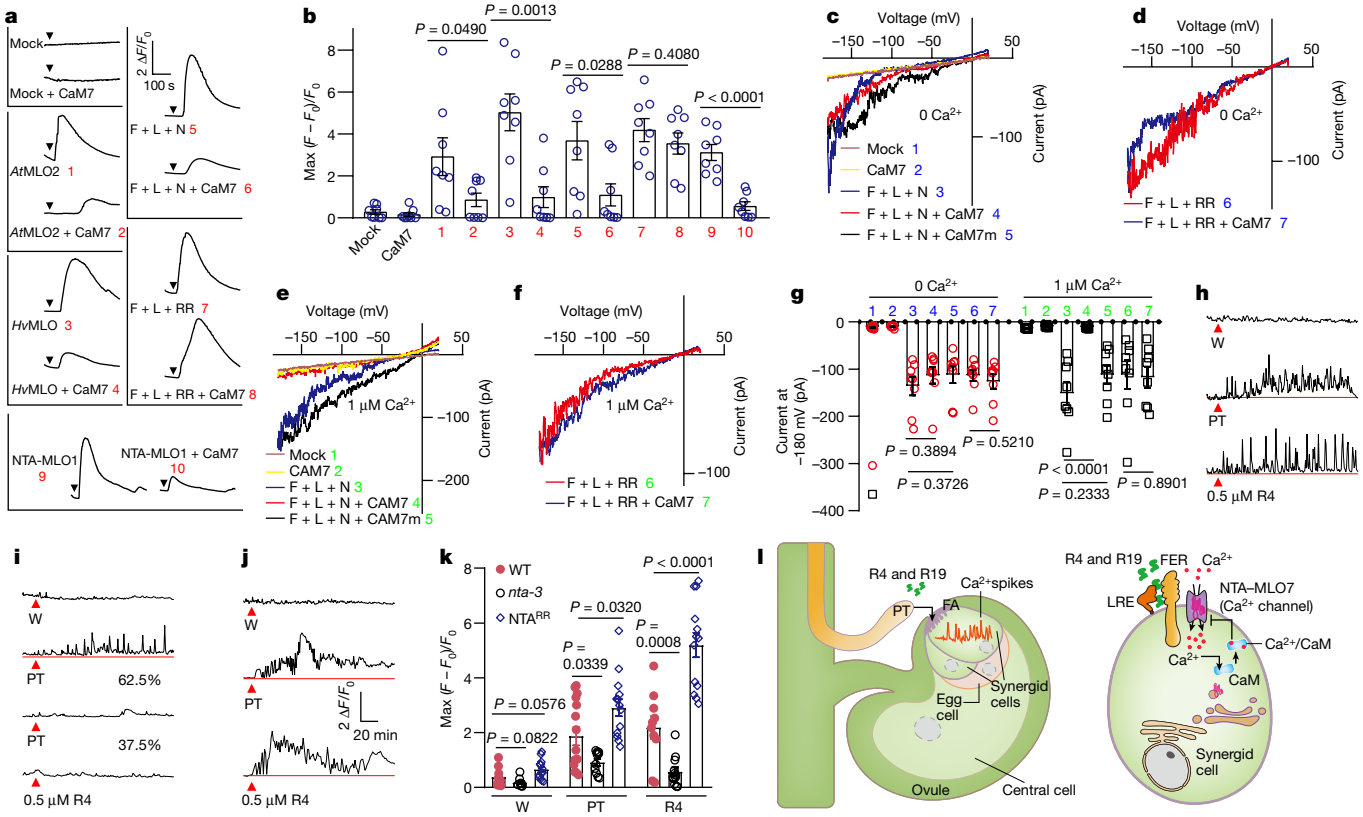

Fig. 4 | CaM inhibition of NTA Ca^{2+} channels is involved in modelling the Ca^{2+} spiking pattern in synergids. a,**b**, Typical Ca^{2+} spiking patterns (**a**) and peak values (**b**) in COS7 cells expressing MLO proteins and *At*CaM7. The arrowheads indicate the time points at which 10 mM external Ca^{2+} was applied. $n = 8$ replicates, and about 60 cells were imaged in each replicate. For **b**, numbers are as indicated for **a** (red). **c**–**f**, Typical whole-cell recordings of inward currents in HEK293T cells expressing the NTA trio, *At*CaM7 or mock cells when $[Ca^{2+}]_{cyt}$ was 0 nM (**c**,**d**) or 1 μM (**e**,**f**). **g**, Current amplitudes at −180 mV of HEK293T cells expressing the NTA trio and *At*CaM7 when $[Ca^{2+}]_{cyt}$ was 0 nM or 1 μM. $n = 8$ cells. Numbers are as indicated in **c**,**d** (blue) and **e**,**f** (green). **h**–**j**, Representative Ca^{2+} spiking patterns in synergids in response to PT arrival or 0.5 μM RALF4 for WT (**h**), *nta-3* (**i**) and NTA^{RR} (**j**). **k**, The peak values of Ca^{2+} spiking as in **h**–**j**. n values are shown in Extended Data Fig. 3. Error bars depict the mean ± s.e.m. All P values were determined by two-tailed Student's t-test. **l**, Model of RALF–FER–LRE–NTA pathway leading to synergid Ca^{2+} changes. Following PT arrival, PT-derived RALF4 and RALF19 bind FER–LRE, and this complex recruits and activates NTA, a CaM-gated Ca^{2+} channel, to initiate Ca^{2+} spiking.

application (Extended Data Fig. 9a). In this mammalian cell system, FER and LRE clearly facilitated the PM localization of NTA (Fig. 2b), which implies that a portion of NTA can be localized in the PM of the synergid in a pollen-tube-independent manner. Following pollen tube arrival, RALF4 and RALF19, and possibly other pollen tube signals (for example, mechanical stimulus), may further activate the Ca^{2+} channel by recruiting the trio to a specific location (for example, the filiform apparatus).

During the revision of this manuscript, five other pollen tube RALFs (RALF6, RALF7, RALF16, RALF36 and RALF37) were reported to bind FER, ANJEA (ANJ) and HERCULES RECEPTOR KINASE 1 (HERK1) and to function redundantly in polytubey block and pollen tube reception[40]. We analysed RALF37 in our assays and found that RALF37, similar to RALF4 and RALF19, also triggered synergid Ca^{2+} changes and activated the NTA trio (Extended Data Fig. 10). This result suggests that multiple RALFs derived from the pollen tube serve as signals to trigger synergid Ca^{2+} spiking, which in turn leads to pollen tube reception. Consistent with this observation, single mutants of *ralf4* and *ralf19* did not show any detectable phenotypic defects (Extended Data Fig. 1b,c).

NTA–CaM shapes synergid Ca^{2+} spiking

MLO proteins contain a CaMBD in the intracellular carboxy-terminal region[30,31], which suggests that these proteins may be regulated by CaM binding, a typical autoregulatory mechanism for many Ca^{2+} channels in both animal and plant systems[41,42]. We examined how CaM affects the channel activity of MLO proteins by co-expressing CaM7 with the NTA trio or other MLO proteins, including *At*MLO2, *Hv*MLO and NTA–MLO1, in COS7 cells. Substantial inhibition of Ca^{2+} entry was observed in all cases (Fig. 4a,b), thereby revealing an inhibitory feedback mechanism of MLO channel activity by CaM. We confirmed this mechanism using a mutant NTA (named NTA^{RR}), in which Leu455 and Trp458 were mutated to Arg to abolish its CaM binding capacity[37]. NTA^{RR} failed to respond to CaM-mediated inhibition (Fig. 4a,b). Although these mutations in the CaMBD partially impaired the redistribution of NTA to the filiform apparatus in the synergid[37], the NTA^{RR} trio was recruited to the PM in COS7 cells (Extended Data Fig. 9b), which is consistent with the finding that the NTA^{RR} trio still conducted Ca^{2+} entry.

As CaM binds to *Hv*MLO in a Ca^{2+}-dependent manner[43], we proposed that CaM may inhibit NTA channel activity following increased $[Ca^{2+}]_{cyt}$ as a negative feedback mechanism. We tested this hypothesis by titrating $[Ca^{2+}]_{cyt}$ and expressing a CaM7 mutant lacking the Ca^{2+}-binding EF motif[44]. The results showed that CaM7 required Ca^{2+} binding to inhibit the activity of the NTA trio (Fig. 4c,e,g). Similarly, the NTA^{RR} mutant (which is defective in CaM binding) became constitutively active (Fig. 4d,f,g). These results support a model in which RALFs activate the NTA channel to increase synergid $[Ca^{2+}]_{cyt}$ to a threshold that in turn enables CaM binding and inhibition of NTA channel activity.

Specific Ca^{2+} spiking in synergids is essential for pollen tube reception[2,3]. We hypothesized that the Ca^{2+}/CaM-dependent feedback inhibition of the NTA channel provides a mechanism for shaping such a Ca^{2+} signature. To test this idea in planta, we generated transgenic plants harbouring the NTA^{RR} mutant driven by the *NTA* promoter in the *nta-3* mutant background

and examined synergid $[Ca^{2+}]_{cyt}$ spikes in response to RALF4. $[Ca^{2+}]_{cyt}$ spiking in synergids was amplified in NTA^{RR} plants (Fig. 4h–k). We also observed higher levels of Ca^{2+} increase in NTA^{RR} synergids in response to pollen tube arrival and a disordered oscillation pattern compared with WT synergids (Fig. 4j,k). This result indicates that the NTA^{RR} mutant, which lacks CaM-dependent inhibition, produces a sustained increase in $[Ca^{2+}]_{cyt}$, which causes a defect in pollen tube reception[37].

Conclusions

We identified pollen-tube-derived RALF peptides as ligands for the FER–LRE co-receptor complex that recruits NTA, a CaM-gated Ca^{2+} channel, to PM domains to initiate Ca^{2+} entry and pollen tube reception (Fig. 4l). This work demonstrated a mechanistic process that integrates the action of FER, LRE and NTA, three players genetically connected in synergid–pollen tube interaction. In addition, the identification of MLO proteins as Ca^{2+} channels uncovered the long sought-after common biochemical pathway (Ca^{2+} entry) that involves MLO functions in multiple physiological processes, including but may not be limited to, mildew resistance, root mechanosensing, pollen tube growth and fertilization in plants. Indeed, Ca^{2+} is a core component in all these processes[11,14], and our finding here sets the stage for extensive future research to address mechanisms in various MLO-dependent processes. As FER–LLG co-receptors are often connected to Ca^{2+} spiking in other signalling processes beyond reproduction[21], the identification of a MLO channel downstream of the FER–LRE co-receptors offers a possible mechanism for other RALF–FER–LLG-dependent pathways. In the context of Ca^{2+} signalling, which is a common theme in all eukaryotes, MLO proteins represent a family of Ca^{2+} channels specific to the plant kingdom, which suggests that instead of having fewer Ca^{2+} channels than animals as currently thought[11], plants may feature channels distinct from animal counterparts and more of these channels await to be discovered.

In the context of reproduction, our study raises several important questions for future research into the mechanistic details of male–female interactions. For example, although RALF4 and RALF19 bind to FER–LRE and enhance the channel activity of NTA, the mechanism underlying this activation awaits resolution by structural analysis of the FER–LRE–NTA trio in the presence of the RALF ligands. Before pollen tube reception, pollen tube integrity and guidance also involve the function of several RALF peptides, FER family of receptor-like kinases and MLO proteins. Our study provides a strategy for further research to link these components in distinct Ca^{2+} signalling pathways. A previous report[34] noted that MLO5 and MLO9 are trafficked together with cyclic nucleotide-gated channel 18 (CNGC18), another Ca^{2+} channel with an essential role in pollen tube growth and guidance. This raises an interesting question regarding the functional interplay of multiple Ca^{2+} channels in shaping specific Ca^{2+} signatures in pollen tubes, synergids and other cell types in plants[42].

Online content

Any methods, additional references, Nature Research reporting summaries, source data, extended data, supplementary information, acknowledgements, peer review information; details of author contributions and competing interests; and statements of data and code availability are available at https://doi.org/10.1038/s41586-022-04923-7.

1. Johnson, M. A., Harper, J. F. & Palanivelu, R. A fruitful journey: pollen tube navigation from germination to fertilization. *Annu. Rev. Plant. Biol.* **70**, 809–837 (2019).
2. Denninger, P. et al. Male–female communication triggers calcium signatures during fertilization in *Arabidopsis*. *Nat. Commun.* **5**, 4645 (2014).
3. Ngo, Q. A., Vogler, H., Lituiev, D. S., Nestorova, A. & Grossniklaus, U. A calcium dialog mediated by the FERONIA signal transduction pathway controls plant sperm delivery. *Dev. Cell* **29**, 491–500 (2014).
4. Escobar-Restrepo, J. M. et al. The FERONIA receptor-like kinase mediates male–female interactions during pollen tube reception. *Science* **317**, 656–660 (2007).
5. Liu, X. et al. The role of LORELEI in pollen tube reception at the interface of the synergid cell and pollen tube requires the modified eight-cysteine motif and the receptor-like kinase FERONIA. *Plant Cell* **28**, 1035–1052 (2016).
6. Kessler, S. A. et al. Conserved molecular components for pollen tube reception and fungal invasion. *Science* **330**, 968–971 (2010).
7. Ge, Z. et al. *Arabidopsis* pollen tube integrity and sperm release are regulated by RALF-mediated signaling. *Science* **358**, 1596–1600 (2017).
8. Blackburn, M. R., Haruta, M. & Moura, D. S. Twenty years of progress in physiological and biochemical investigation of RALF peptides. *Plant Physiol.* **182**, 1657–1666 (2020).
9. Clapham, D. E. Calcium signaling. *Cell* **131**, 1047–1058 (2007).
10. Trewavas, A. Le calcium, c'est la vie: calcium makes waves. *Plant Physiol.* **120**, 1–6 (1999).
11. Luan, S. & Wang, C. Calcium signaling mechanisms across kingdoms. *Annu. Rev. Cell Dev. Biol.* **37**, 311–340 (2021).
12. Hwang, J. Y. et al. Dual sensing of physiologic pH and calcium by EFCAB9 regulates sperm motility. *Cell* **177**, 1480–1494.e19 (2019).
13. Whitaker, M. Calcium at fertilization and in early development. *Physiol. Rev.* **86**, 25–88 (2006).
14. Chen, J., Gutjahr, C., Bleckmann, A. & Dresselhaus, T. Calcium signaling during reproduction and biotrophic fungal interactions in plants. *Mol. Plant* **8**, 595–611 (2015).
15. Hamamura, Y. et al. Live imaging of calcium spikes during double fertilization in *Arabidopsis*. *Nat. Commun.* **5**, 4722 (2014).
16. Iwano, M. et al. Cytoplasmic Ca^{2+} changes dynamically during the interaction of the pollen tube with synergid cells. *Development* **139**, 4202–4209 (2012).
17. Ge, Z., Dresselhaus, T. & Qu, L. J. How CrRLK1L receptor complexes perceive RALF signals. *Trends Plant. Sci.* **24**, 978–981 (2019).
18. Franck, C. M., Westermann, J. & Boisson-Dernier, A. Plant malectin-like receptor kinases: from cell wall integrity to immunity and beyond. *Annu. Rev. Plant Biol.* **69**, 301–328 (2018).
19. Li, C. et al. Glycosylphosphatidylinositol-anchored proteins as chaperones and co-receptors for FERONIA receptor kinase signaling in *Arabidopsis*. *eLife* **4**, e06587 (2015).
20. Cheung, A. Y., Qu, L. J., Russinova, E., Zhao, Y. & Zipfel, C. Update on receptors and signaling. *Plant Physiol.* **182**, 1527–1530 (2020).
21. Haruta, M., Sabat, G., Stecker, K., Minkoff, B. B. & Sussman, M. R. A peptide hormone and its receptor protein kinase regulate plant cell expansion. *Science* **343**, 408–411 (2014).
22. Stegmann, M. et al. The receptor kinase FER is a RALF-regulated scaffold controlling plant immune signaling. *Science* **355**, 287–289 (2017).
23. Xiao, Y. et al. Mechanisms of RALF peptide perception by a heterotypic receptor complex. *Nature* **572**, 270–274 (2019).
24. Ge, Z. et al. LLG2/3 are co-receptors in BUPS/ANX-RALF signaling to regulate *Arabidopsis* pollen tube integrity. *Curr. Biol.* **29**, 3256–3265.e5 (2019).
25. Liu, C. et al. Pollen PCP-B peptides unlock a stigma peptide–receptor kinase gating mechanism for pollination. *Science* **372**, 171–175 (2021).
26. Zhou, X. et al. Membrane receptor-mediated mechano-transduction maintains cell integrity during pollen tube growth within the pistil. *Dev. Cell* **56**, 1030–1042.e6 (2021).
27. Liu, K. H. et al. Discovery of nitrate–CPK–NLP signalling in central nutrient–growth networks. *Nature* **545**, 311–316 (2017).
28. Kasahara, R. D., Portereiko, M. F., Sandaklie-Nikolova, L., Rabiger, D. S. & Drews, G. N. MYB98 is required for pollen tube guidance and synergid cell differentiation in *Arabidopsis*. *Plant Cell* **17**, 2981–2992 (2005).
29. Buschges, R. et al. The barley *Mlo* gene: a novel control element of plant pathogen resistance. *Cell* **88**, 695–705 (1997).
30. Devoto, A. et al. Molecular phylogeny and evolution of the plant-specific seven-transmembrane MLO family. *J. Mol. Evol.* **56**, 77–88 (2003).
31. Kusch, S., Pesch, L. & Panstruga, R. Comprehensive phylogenetic analysis sheds light on the diversity and origin of the MLO family of integral membrane proteins. *Genome Biol. Evol.* **8**, 878–895 (2016).
32. Chen, Z. et al. Two seven-transmembrane domain MILDEW RESISTANCE LOCUS O proteins cofunction in *Arabidopsis* root thigmomorphogenesis. *Plant Cell* **21**, 1972–1991 (2009).
33. Consonni, C. et al. Conserved requirement for a plant host cell protein in powdery mildew pathogenesis. *Nat. Genet.* **38**, 716–720 (2006).
34. Meng, J. G. et al. Integration of ovular signals and exocytosis of a Ca^{2+} channel by MLOs in pollen tube guidance. *Nat. Plants* **6**, 143–153 (2020).
35. Pan, Y. et al. Dynamic interactions of plant CNGC subunits and calmodulins drive oscillatory Ca^{2+} channel activities. *Dev. Cell* **48**, 710–725.e5 (2019).
36. Jones, D. S. et al. MILDEW RESISTANCE LOCUS O function in pollen tube reception is linked to its oligomerization and subcellular distribution. *Plant Physiol.* **175**, 172–185 (2017).
37. Ju, Y. et al. Polarized NORTIA accumulation in response to pollen tube arrival at synergids promotes fertilization. *Dev. Cell* **56**, 2938–2951.e6 (2021).
38. Kessler, S. A., Lindner, H., Jones, D. S. & Grossniklaus, U. Functional analysis of related CrRLK1L receptor-like kinases in pollen tube reception. *EMBO Rep.* **16**, 107–115 (2015).
39. Haruta, M., Gaddameedi, V., Burch, H., Fernandez, D. & Sussman, M. R. Comparison of the effects of a kinase-dead mutation of FERONIA on ovule fertilization and root growth of *Arabidopsis*. *FEBS Lett.* **592**, 2395–2402 (2018).
40. Zhong, S. et al. RALF peptide signaling controls the polytubey block in *Arabidopsis*. *Science* **375**, 290–296 (2022).
41. Ben-Johny, M. & Yue, D. T. Calmodulin regulation (calmodulation) of voltage-gated calcium channels. *J. Gen. Physiol.* **143**, 679–692 (2014).
42. Tian, W., Wang, C., Gao, Q., Li, L. & Luan, S. Calcium spikes, waves and oscillations in plant development and biotic interactions. *Nat. Plants* **6**, 750–759 (2020).
43. Kim, M. C. et al. Calmodulin interacts with MLO protein to regulate defence against mildew in barley. *Nature* **416**, 447–451 (2002).
44. Tian, W. et al. A calmodulin-gated calcium channel links pathogen patterns to plant immunity. *Nature* **572**, 131–135 (2019).

Methods

Plant material and growth conditions

Seeds were sterilized with 10% (v/v) bleach and sown on agar plates containing half-strength Murashige and Skoog (1/2 MS) medium (1/2 MS, 0.8% (w/v) Phyto agar and 1% (w/v) sucrose, pH adjusted to 5.8 with KOH). Plates were incubated at 4 °C for 3 days for stratification and then transferred to the soil pots in a 22 °C growth room with a 16-h light/8-h dark cycle (100 μmol m^{-2} s^{-1}). The seeds for *fer-4* (GABI_GK106A06), *lre-5* (CS66102) and *nta-3* (SALK_027128) were purchased from *Arabidopsis* Biological Resource Center. The *ralf4* and *ralf19* mutants were generated by CRISPR as previously reported[7].

Transgenic plants

The coding DNA sequence (CDS) of GCaMP6s was PCR-amplified using HBT-GCaMP6-HA as the template[27] and fused to the *MYB98* promoter region[28], amplified from Columbia-0 (Col-0) genomic DNA in the pCAMBIA 2300 vector. The binary construct was transformed into *Arabidopsis thaliana* (Col-0) plants through *Agrobacterium* (GV3101) using the floral dip method[45]. Transgenic plants were selected on 1/2 MS plates containing 50 mg l^{-1} kanamycin, and one homozygous transgenic p*MYB98-GCaMP6s* line was then crossed with *fer-4*, *lre-5* and *nta-3* and further brought to homozygosity with both the GCaMP6s and the *fer-4*, *lre-5* and *nta-3* genetic backgrounds. The NTA^{RR} mutant was produced by site-directed mutagenesis to replace Leu455 and Trp458 with Arg. The *NTA* promoter was PCR-amplified from Col-0 genomic DNA and fused with the NTA^{RR} CDS in the pCAMBIA 1305 vector and transformed into plants as described above.

β-Glucuronidase staining

The mature pistils of the transgenic plants carrying pro*RALF4*/*19*:β-glucuronidase (GUS) were dissected to isolate intact ovules that were then fixed in 80% acetone overnight. Samples were then incubated with GUS staining buffer (50 mM sodium phosphate, pH 7.2, 2 mM potassium ferrocyanide, 2 mM potassium ferricyanide, 0.2% Triton X-100 and 2 mM X-Gluc). Images were taken with a Zeiss AxioObserver Z1 inverted microscope.

Aniline blue staining

Pollen grains of a freshly opened flower of WT or mutant lines were used to pollinate WT pistils that had been emasculated a day earlier. After 24 h, the pistils were fixed in acetic acid/ethanol (1:3) overnight. They were then washed stepwise in 70% ethanol, 50% ethanol, 20% ethanol and ddH_2O. The pistils were treated with 8 M NaOH overnight to soften the tissues and then washed with ddH_2O three times before staining with aniline blue solution (0.1% aniline blue, 50 mM K_3PO_4) for 2 h. The stained pistils were observed using a Zeiss AxioObserver Z1 inverted microscope.

Mammalian cell culture, vector construction and transfection

The CDS of GCaMP6s was amplified from HBT-GCaMP6-HA[27] and cloned into a dual-promoter vector, pBudCE4.1 (Invitrogen), with each CDS for NTA, FER, LRE, NTA–MLO1 for co-expression in HEK293T or COS7 cells. The chimeric NTA–MLO1 CDS was generated as previously described[36].

Mammalian cells were cultured in DMEM supplemented with 10% FBS in a 5% CO_2 incubator at 37 °C with controlled humidity. HEK293T or COS7 cells were transfected using a Lipofectamine 3000 Transfection Reagent kit (Invitrogen). Plasmids for transfection were extracted from *Escherichia coli* (DH5α) using a Plasmid Mini kit (Qiagen), and 2 μg plasmid DNA was added into each well of 6-well plates (Nunc) containing the cells (70–80% confluent). To confirm that the cells were successfully transfected, green and/or red fluorescence signals were examined using an inverted fluorescence microscope (Zeiss AxioObserver Z1 inverted microscope) before patch-clamp and Ca^{2+} imaging experiments 48 h after transfection.

Whole-cell patch-clamp recording

The whole-cell patch-clamp experiments were performed using an Axopatch-200B patch-clamp setup (Axon Instruments) with a Digitata1550 digitizer (Axon Instruments) as previously described[46]. Clampex10.7 software (Axon Instruments) was used for data acquisition, and Clampfit 10.7 was used for data analysis.

To record Ca^{2+} currents across the PM of HEK293T cells, the standard bath solution contained 140 mM *N*-methyl-D-glucamine (NMDG)-Cl, 10 mM $CaCl_2$, 10 mM glucose and 10 mM HEPES, adjusted to pH 7.2 with $Ca(OH)_2$. The standard pipette solution contained 140 mM Cs-glutamate, 6.7 mM EGTA, 3.35 mM $CaCl_2$ and 10 mM HEPES, adjusted to pH 7.2 with CsOH. Free [Ca^{2+}] in the pipette solution was 175 nM, as calculated using the Webmaxc Standard (https://somapp.ucdmc.ucdavis.edu/pharmacology/bers/maxchelator/webmaxc/webmaxcS.htm). The 10 mM Ca^{2+} in the bath solution was removed to attain 0 mM Ca^{2+} or substituted with 10 mM Ba^{2+} or 10 mM Mg^{2+} as indicated. A ramp voltage protocol of 2-s duration from −160 mV to +30 mV (holding potential 0 mV) was applied 1 min after achieving a whole-cell configuration, and currents were recorded every 20 s, with 5 repeats in total for each cell. The five current traces were used for statistical analysis to produce average current–voltage curves.

For inward K^+ current recordings in HEK293T cells, the bath solution contained 140 mM NMDG-Cl, 14.5 mM KCl, 10 mM glucose and 10 mM HEPES, adjusted to pH 7.2 with KOH. The pipette solution contained 145 mM K-glutamate, 3.35 mM EGTA, 1.675 mM $CaCl_2$ and 10 mM HEPES, adjusted to pH 7.2 with KOH. The free [Ca^{2+}] in the pipette solution was 100 nM, as calculated using the Webmaxc Standard.

For inward Na^+ current recordings in HEK293T cells, the bath solution contained 140 mM NaCl, 10 mM glucose and 10 mM HEPES, adjusted to pH 7.2 with NaOH. The pipette solution contained 135 mM CsCl, 10 mM NaCl, 3.35 mM EGTA, 1.675 mM $CaCl_2$ and 10 mM HEPES, adjusted to pH 7.2 with CsOH. The free [Ca^{2+}] in the pipette solution was 100 nM, as calculated using the Webmaxc Standard.

A step voltage protocol of 4-s duration for each voltage from −160 mV to +60 mV with a +20 mV increment was used for K^+ and Na^+ current recordings in HEK293T cells 1 min after achieving a whole-cell configuration.

Two-electrode voltage-clamp recording from *Xenopus* oocytes

The CDS for NTA-3×HA, LRE-4×Myc and FER-3×Flag were cloned into the pGEMHE *Xenopus* oocyte expression vector. To construct LRE-4×Myc, the 4×Myc tag sequence was inserted after the first 60 bp of the LRE CDS encoding the signal peptide, followed by the downstream 438 bp of LRE as previously described[23].

Two-electrode voltage-clamp assays were performed as previously reported[35,44]. The capped RNA (cRNA) was synthesized from 1 μg of a linearized plasmid DNA template using a mMESSAGE mMACHINE T7 kit (Ambion) and 10 ng of each cRNA, in a total volume of 46 nl, was injected into each oocyte. Injected oocytes were incubated in ND96 solution (96 mM NaCl, 2 mM KCl, 1 mM $MgCl_2$, 1.8 mM $CaCl_2$, 10 mM HEPES/NaOH, pH 7.4) at 18 °C for 2 days before electrophysiological recording. Oocytes were voltage-clamped using a TEV 200A amplifier (Dagan), a Digidata 1550 A/D converter, and recorded using CLAMPex 10.7 software (Axon Instruments). The pipette solution contained 3 M KCl. The standard bath solution contained 30 mM $CaCl_2$, 1 mM KCl, 2 mM NaCl, 130 mM mannitol and 5 mM MES-Tris (pH 5.5). Voltage steps were applied from +40 mV to −160 mV in −20 mV decrements over 0.8 s.

Single-cell Ca^{2+} imaging in mammalian cells

HEK293T or COS7 cells expressing GCaMP6s and various combinations of candidate channel proteins were monitored using a Zeiss AxioObserver Z1 inverted microscope (Ivision 4.5 software) with a ×20 objective as previously reported[35]. The interval of data acquisition was 2 s. The standard solution for Ca^{2+} imaging contained 120 mM NaCl,

3 mM KCl, 1 mM $MgCl_2$, 1.2 mM $NaHCO_3$, 10 mM glucose, 10 mM HEPES, pH 7.5. About 60 s after initiation of the imaging procedure, the bath was perfused using a peristaltic pump with the standard solution supplemented with 10 mM Ca^{2+} and/or RALFs to elicit Ca^{2+} entry through active channels.

Synergid cell Ca^{2+} imaging

For the RALF-induced synergid $[Ca^{2+}]_{cyt}$ increase experiment, unfertilized ovules were dissected from flowers as previously described[47]. The pistil was dissected to remove the ovules from the placenta using a surgical needle. The isolated ovules were placed in pollen germination medium (PGM), which contained 18% sucrose, 0.01% boric acid, 1 mM $MgSO_4$, 1 mM $CaCl_2$, 1 mM $Ca(NO_3)_2$ and 0.5% agarose (pH 7.0)[48]. After 2 h of incubation at 22 °C and 100% relative humidity, synergids expressing GCaMP6s were monitored using a Zeiss AxioObserver Z1 inverted microscope (Ivision 4.5 software) with a ×20 objective, and various RALFs were added to the ovules as indicated.

For the pollen-tube-induced synergid $[Ca^{2+}]_{cyt}$ increase experiment, we followed a previously published protocol[2,3]. Dissected ovules of emasculated flowers expressing GCaMP6s were placed on PGM. Unpollinated pistils were cut with a razor blade (VWR International) at the junction between the style and ovary. The stigmas were placed on the PGM and manually pollinated with pollen grains expressing DsRed. Pollinated stigmas were positioned 150 µm away from the ovules, and pollen tube growth was monitored using a fluorescence microscope. Time-lapse Ca^{2+} imaging began after the pollen tube entered the ovule micropyle.

Protein localization

Transfected COS7 cells were washed with PBS and mounted onto slides for image acquisition with a Zeiss LSM 880 confocal microscope and ZEN2012 software.

Peptide purification

All tag-free RALF peptides used in this study were purified from insect cells (High 5). The pFastBac vector containing RALF4, RALF19 and LRX8 were gifts from J. Santiago (University of Lausanne), and RALF4 and RALF19 peptides were purified as previously reported[49].

For RALF8, RALF9, RALF15, RALF25, RALF26, RALF30 and RALF34, the CDS encoding RALF mature peptides were cloned into a modified pACEBAC1 (Geneva Biotech) vector in which RALFs were amino-terminally fused to a 30K signal peptide, a 10×His tag, thioredoxin A and a tobacco etch virus (TEV) protease site.

High 5 cells were infected with virus with a multiplicity of infection of 3 and incubated for 1 day at 28 °C and 2 days at 22 °C at 110 r.p.m. on an orbital shaker. The secreted peptides were purified from the supernatant with a Ni^{2+} column (Ni-NTA, Qiagen), and incubated with TEV protease (NEB) to remove the tags. Peptides were further purified by size-exclusion chromatography on a Superdex 200 increase 10/300 GL column (GE Healthcare), equilibrated in 20 mM sodium citrate, pH 5.0, 150 mM NaCl. The peptides were diluted with sterile pure water before use.

Protein–protein interaction assays

For pull-down assays, MBP–FER_{ex}, GST–RALFs and GST–LRE were produced in *E. coli* Rosetta (DE3) by 0.1 mM IPTG induction overnight at 16 °C and bound to amylose or glutathione resins for purification as previously reported[19,50]. The pull-down buffer contained 40 mM Tris–HCl, pH 7.5, 100 mM NaCl, 1 mM EDTA, 5% glycerol, 5 mM $MgCl_2$, 1 mM PMSF, complete protease inhibitor cocktail (Roche) at 1:100 dilution, and 0.4% Triton X-100. Proteins were applied to amylose resin and incubated at 4 °C for 2 h with gentle mixing. The resin was washed three times in pull-down buffer. Proteins that remained bound to the resin were eluted by mixing with SDS–PAGE loading buffer, boiled for 5 min and subjected to 12% SDS–PAGE and western blotting.

For co-IP of tobacco leaves, 35S:FERK565R–3×Flag and 35S:LRE–4Myc constructs were co-transformed into *Agrobacterium tumefaciens* (strain GV3101) and infiltrated into *N. benthamiana* leaves[23]. Sixty hours after inoculation, leaves were detached and treated with 5 µM RALFs for 2 h before total protein was extracted and applied to anti-Flag M2 affinity agarose gel (Sigma-Aldrich). After incubation at 4 °C for 2 h with gentle mixing, the resin was washed three times in pull-down buffer, and the bound protein was eluted by mixing with SDS–PAGE loading buffer, boiled for 5 min and subjected to 10% SDS–PAGE and western blotting.

For co-IP of *Xenopus* oocytes, cRNAs of FER–3×Flag, NTA–3HA and LRE–4Myc were injected into oocytes, incubated for 3 days, followed by treatment with 5 µM RALFs for 2 h. Total protein was extracted in the pull-down buffer and then applied to anti-Flag M2 affinity agarose gel (Sigma-Aldrich). After incubation at 4 °C for 2 h with gentle mixing, the resin was washed three times in pull-down buffer, and the bound protein was eluted by mixing with SDS–PAGE loading buffer, boiled for 5 min and subjected to 10% SDS–PAGE and western blotting.

For chemiluminescence detection, the following antibodies were used: anti-GST–HRP (1: 2,000 dilution), anti-Myc–HRP (1: 2,000 dilution), anti-HA (1: 2,000 dilution), anti-MBP (1: 2,000 dilution) and anti-mouse secondary (1:20,000 dilution) antibodies from Santa Cruz Biotechnology; and anti-Flag antibody (1:4,000 dilution) from Sigma-Aldrich.

Image processing and data analysis

ImageJ (v.1.51j8) was used to analyse GCaMP6s signals over time at several regions of interest. To calculate the fractional fluorescence change ($\Delta F/F$), the equation $\Delta F/F = (F - F_0)/F_0$ was used, where F_0 denotes the average baseline fluorescence determined by the average of F over the first 10 frames of the recording before the treatment.

Microsoft Excel in Office 365 and GraphPad Prism 7.0 were used for calculation and statistical analyses of the data. Adobe Illustrator CC 2019 was used for image assembly. Clampfit 10.7 was used to analyse and process data from the electrophysiological experiments. All experiments were independently reproduced in the laboratory.

Reporting summary

Further information on research design is available in the Nature Research Reporting Summary linked to this paper.

Data availability

The data supporting the findings of this study are available within the paper and its Supplementary Information files. Source data are provided with this paper.

45. Clough, S. J. & Bent, A. F. Floral dip: a simplified method for *Agrobacterium*-mediated transformation of *Arabidopsis thaliana*. *Plant J.* **16**, 735–743 (1998).
46. Gao, Q. F. et al. Cyclic nucleotide-gated channel 18 is an essential Ca^{2+} channel in pollen tube tips for pollen tube guidance to ovules in *Arabidopsis*. *Proc. Natl Acad. Sci. USA* **113**, 3096–3101 (2016).
47. Palanivelu, R. & Preuss, D. Distinct short-range ovule signals attract or repel *Arabidopsis thaliana* pollen tubes in vitro. *BMC Plant Biol.* **6**, 7 (2006).
48. Li, H. et al. Control of pollen tube tip growth by a Rop GTPase-dependent pathway that leads to tip-localized calcium influx. *Plant Cell* **11**, 1731–1742 (1999).
49. Moussu, S. et al. Structural basis for recognition of RALF peptides by LRX proteins during pollen tube growth. *Proc. Natl Acad. Sci. USA* **117**, 7494–7503 (2020).
50. Duan, Q. et al. FERONIA receptor-like kinase regulates RHO GTPase signaling of root hair development. *Proc. Natl Acad. Sci. USA* **107**, 17821–17826 (2010).

Acknowledgements We thank J. Santiago of the University of Lausanne for providing the pFastBac-RALF4/19 and LRX8 vector; B. Li of UC Berkeley for advice on protein purification from insect cells; R. Palanivelu of the University of Arizona for providing p*LAT52*:DsRed seeds; and S. Ruzin and D. Schichnes at The Biological Imaging Facility of UC Berkeley for their assistance.

Author contributions Q.G., C.W., L.L. and S.L. conceived and designed the experiments. Q.G., Y.X. and Q.S. performed the molecular cloning and biochemical experiments and generated the transgenic plants. Q.G. performed the patch-clamp and voltage clamp recordings and Ca^{2+} imaging. Q.G., C.W. and S.L. wrote the manuscript. All authors discussed the results and commented on the manuscript.

Competing interests The authors declare no competing interests.

Additional information

Supplementary information The online version contains supplementary material available at https://doi.org/10.1038/s41586-022-04923-7.

Correspondence and requests for materials should be addressed to Sheng Luan.

Peer review information *Nature* thanks the anonymous reviewers for their contribution to the peer review of this work.

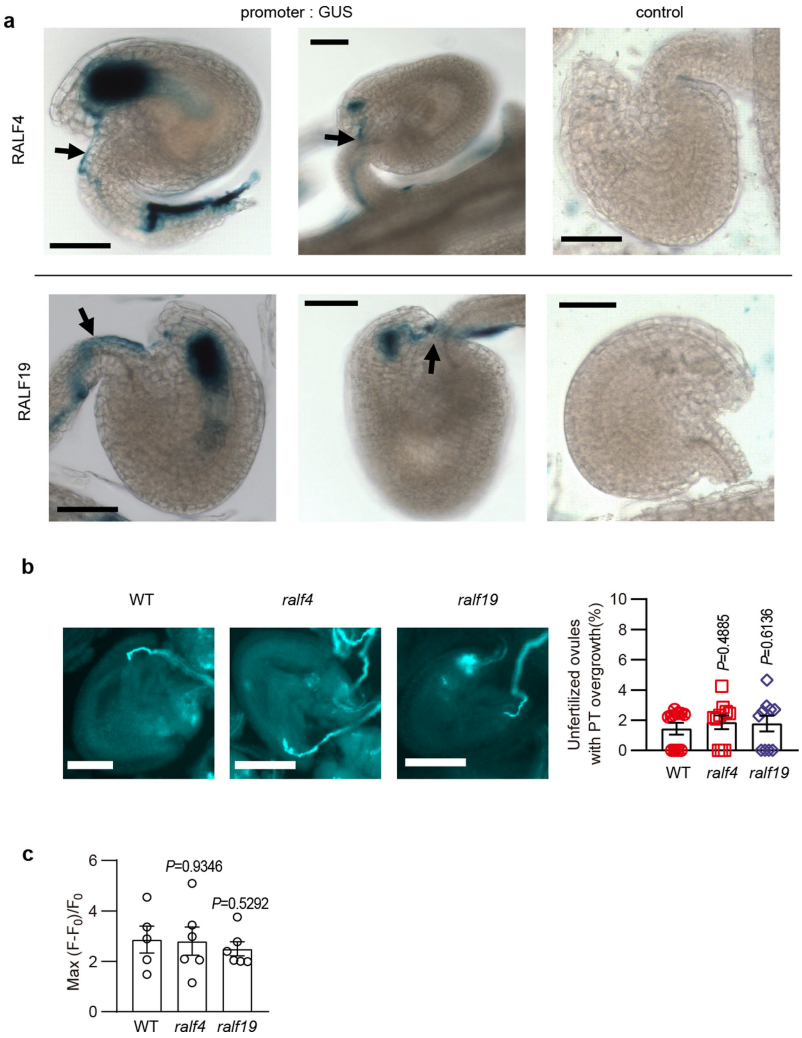

Extended Data Fig. 1 | Expression and redundant function of RALF4 and 19 in pollen tube reception. a, Expression pattern of RALF4 and 19 during pollen tube reception. Arrows indicated pollen tubes (from pro*RALF*-GUS plants) that penetrated ovules (pro*RALF*-GUS plants). For control, pollen grains from non-transgenic plants were used to pollinate the promoter: GUS transgenic plants, showing no expression of GUS in the ovule. **b**, *ralf4* and *ralf19* single mutants did not show pollen tube overgrowth. n = 10 pistils. **c**, The peak values of the synergid Ca^{2+} spikes triggered by pollen tubes of *ralf4* and *ralf19* single mutants was similar to that of WT. n = 5 ovules for WT, and n = 6 ovules for *ralf4* and *ralf19*. Bar, 50 μm. Error bars depict means ± S.E.M. All *P* values were determined by two-tailed Student's *t*-test.

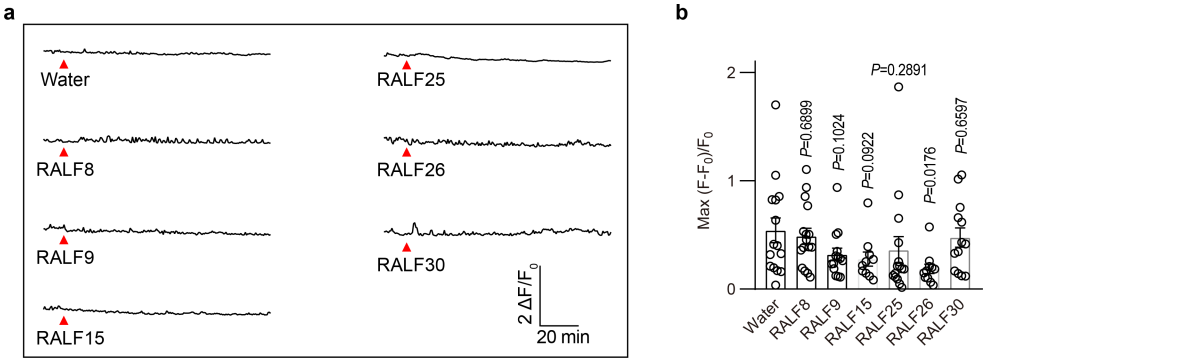

Extended Data Fig. 2 | RALF8, 9, 15, 25, 26 and 30 failed to induce synergid Ca^{2+} changes. a, Representative Ca^{2+} spiking patterns in synergid cells in response to 0.5 μM RALFs. **b**, The peak values of Ca^{2+} spiking as in (**a**). n = 15 ovules for water treatment, n = 16 ovules for RALF8, n = 14 ovules for RALF9, n = 10 ovules for RALF15, n = 15 ovules for RALF25, n = 11 ovules for RALF26 and n = 13 ovules for RALF30. Error bars depict means ± S.E.M. All *P* values were determined by two-tailed Student's *t*-test.

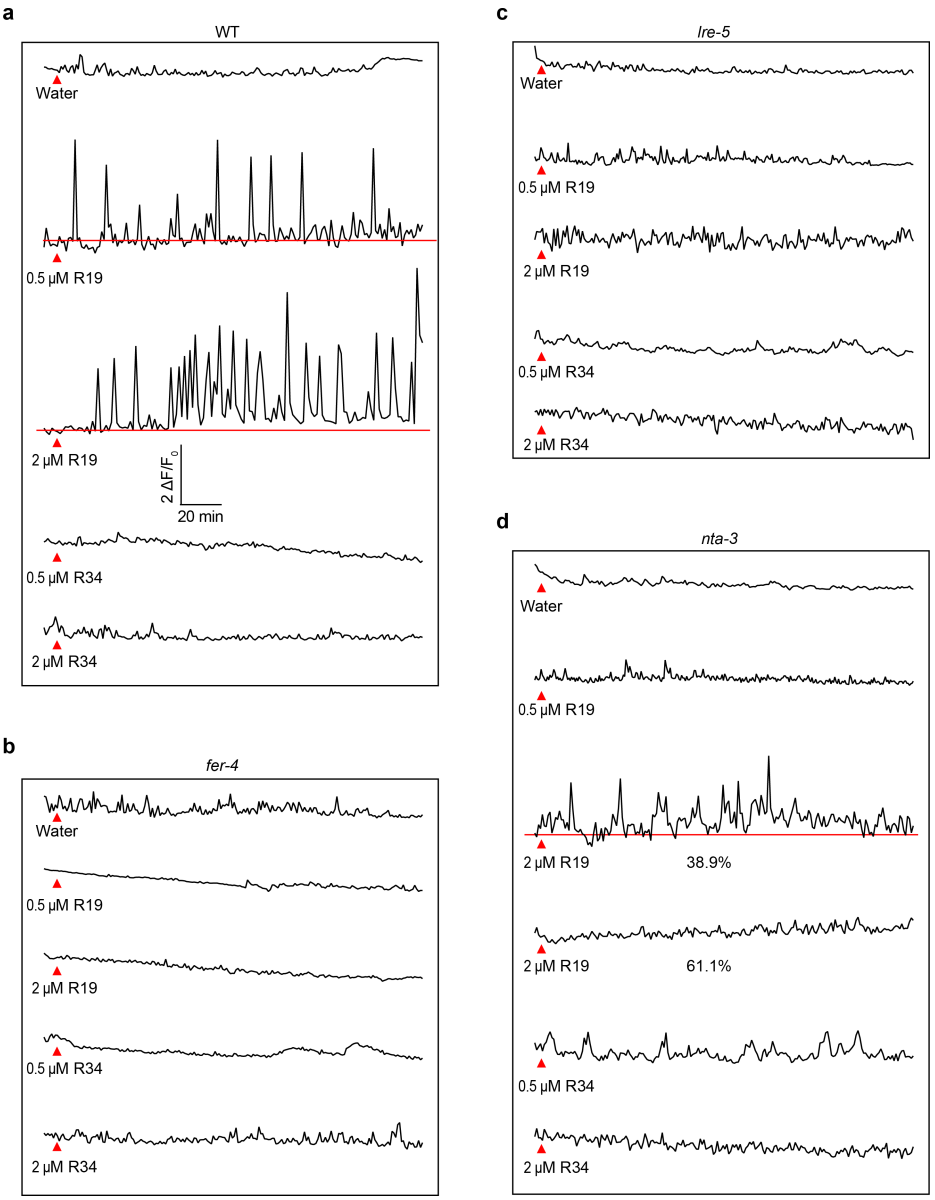

Extended Data Fig. 3 | Pollen tube derived RALF4/19 induce synergid Ca^{2+} oscillations. Representative Ca^{2+} spiking patterns in synergid cells in response to 0.5 μM and 2 μM RALF19 or RALF34 for WT (**a**), *fer-4* (**b**), *lre-5* (**c**) and *nta-3* (**d**). Red triangles indicate time points at which RALFs was applied. In Fig. 1i, for water treatment, n = 13 ovules for WT, n = 11 ovules for *fer-4*, n = 11 ovules for *lre-5*, and n = 11 ovules for *nta-3*; for pollen tube, n = 13 ovules for WT, n = 17 ovules for *fer-4*, n = 7 ovules for *lre-5* and n = 10 ovules for *nta-3*; for 0.5 μM RALF4 treatment, n = 12 ovules for WT, n = 15 ovules for *fer-4*, n = 13 ovules for *lre-5* and n = 13 ovules for *nta-3*; For 2 μM RALF4 treatment, n = 11 ovules for WT, n = 10 ovules for *fer-4*, n = 13 ovules for *lre-5* and n = 14 ovules for *nta-3*; For 0.5 μM RALF19 treatment, n = 13 ovules for WT, n = 10 ovules *fer-4*, n = 11 ovules for *lre-5* and n = 12 ovules *nta-3*. For 2 μM RALF19 treatment, n = 11 ovules for WT, n = 10 ovules for *fer-4*, n = 12 ovules for *lre-5* and n = 14 ovules for *nta-3*; For 0.5 μM RALF34 treatment, n = 11 ovules for WT, n = 12 ovules for *fer-4*, n = 12 ovules for *lre-5* and n = 13 ovules for *nta-3*; For 2 μM RALF34 treatment, n = 10 ovules for WT, n = 11 ovules for *fer-4*, n = 12 ovules for *lre-5* and n = 14 ovules for *nta-3*. In Fig. 4k, in WT n = 14 ovules for water treatment, n = 15 ovules for pollen tube and n = 10 ovules for 0.5 μM RALF4 treatment; in *nta-3*, n = 11 ovules for water treatment, n = 10 ovules for pollen tube and n = 12 ovules 0.5 μM RALF4; in NTA^{RR}, n = 13 ovules for water treatment, n = 14 ovules for pollen tube and n = 13 ovules for 0.5 μM RALF4.

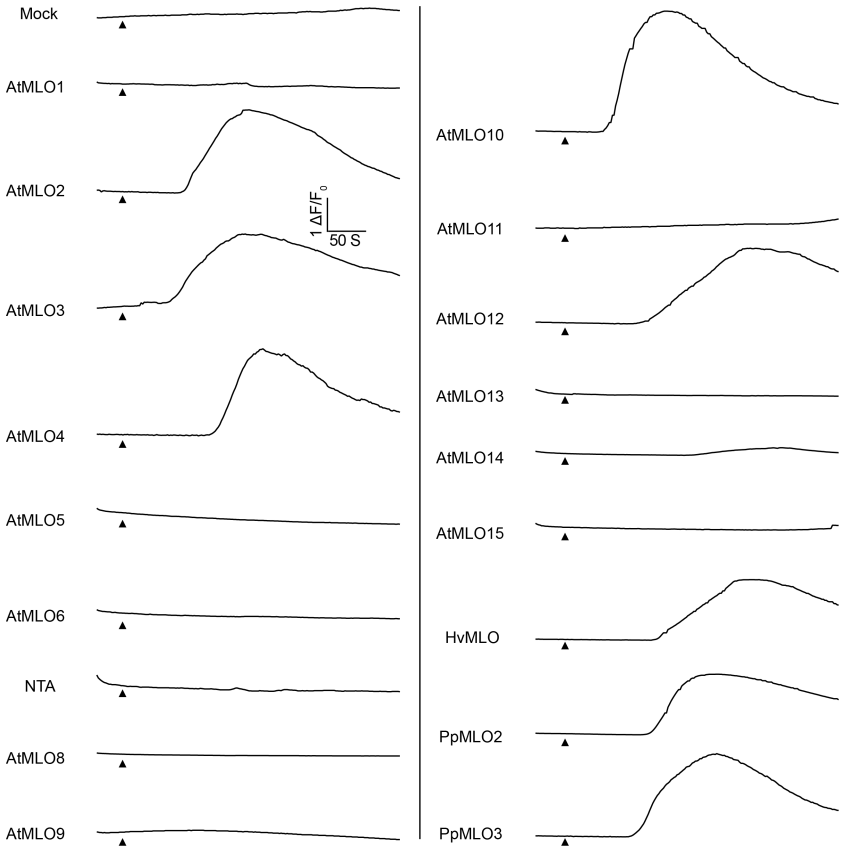

Extended Data Fig. 4 | Representative cytosolic Ca^{2+} increase curves of COS7 cells expressing various MLOs. The black triangle indicated the time point when 10 mM external Ca^{2+} was applied.

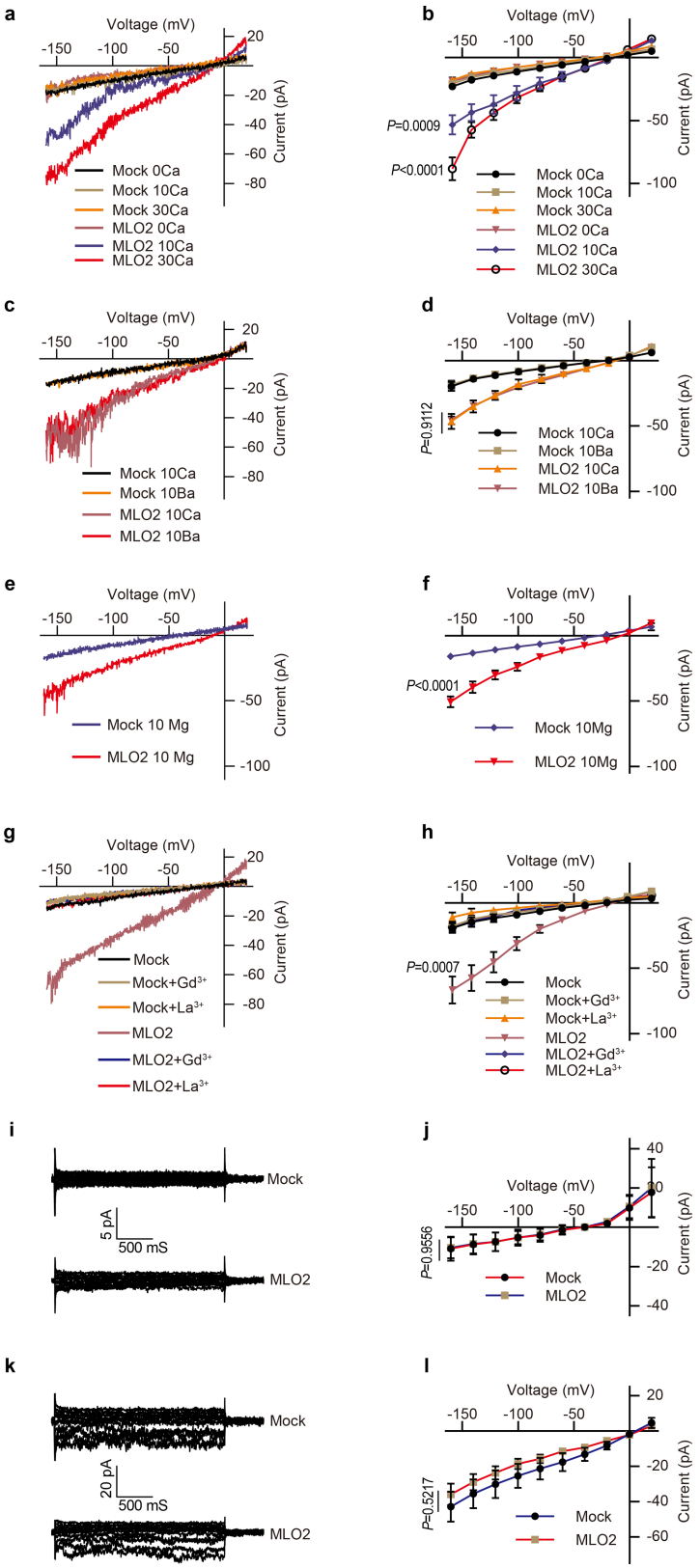

Extended Data Fig. 5 | Conductivity of *At*MLO2 to divalent and monovalent cations. (**a**) Typical whole-cell recordings and (**b**) average current-voltage curves of the inward currents showing external Ca^{2+} dependence (0 mM, 10 mM and 30mM) in HEK293T cells expressing *At*MLO2. (**c**) Typical whole-cell recordings and (**d**) average current-voltage curves for Ba^{2+} conductance by *At*MLO2 in HEK293T cells. (**e**) Typical whole-cell recordings and (**f**) average current-voltage curves for Mg^{2+} conductance by *At*MLO2 in HEK293T cells. (**g**) Typical whole-cell recordings and (**h**) average current-voltage curves for Gd^{3+} (100 μM) and La^{3+} (100 μM) inhibition of Ca^{2+} conductance in HEK293T cells expressing *At*MLO2. (**i**) Typical whole-cell recordings and (**j**) average current-voltage curves of the inward currents showing no detectable K^+ conductance by *At*MLO2 in HEK293T cells. (**k**) Typical whole-cell recordings and (**l**) average current-voltage curves of the inward currents showing no detectable Na^+ conductance by *At*MLO2 in HEK293T cells. Error bars depict means ± S.E.M. n values = 8 cells. All *P* values were determined by two-tailed Student's *t*-test.

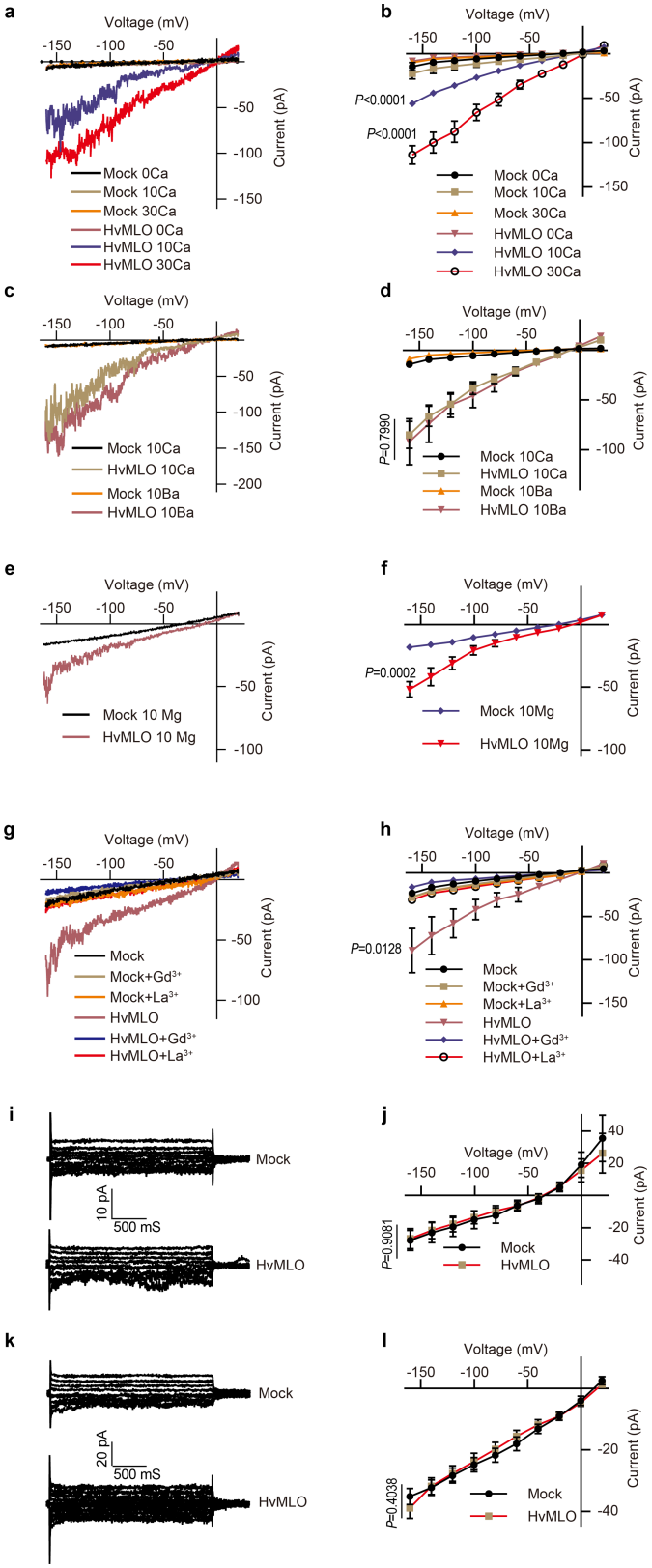

Extended Data Fig. 6 | See next page for caption.

Extended Data Fig. 6 | Conductivity of *Hv*MLO to divalent and monovalent cations. (**a**) Typical whole-cell recordings and (**b**) average current-voltage curves of the inward currents showing external Ca^{2+} dependence (0 mM, 10 mM and 30mM) in HEK293T cells expressing *Hv*MLO. (**c**) Typical whole-cell recordings and (**d**) average current-voltage curves for Ba^{2+} conductance by *Hv*MLO in HEK293T cells. (**e**) Typical whole-cell recordings and (**f**) average current-voltage curves for Mg^{2+} conductance by *Hv*MLO in HEK293T cells. (**g**) Typical whole-cell recordings and (**h**) average current-voltage curves for Gd^{3+} (100 µM) and La^{3+} (100 µM) inhibition of Ca^{2+} conductance in HEK293T cells expressing *Hv*MLO. (**i**) Typical whole-cell recordings and (**j**) average current-voltage curves of the inward currents showing no detectable K^+ conductance by *Hv*MLO in HEK293T cells. (**k**) Typical whole-cell recordings and (**l**) average current-voltage curves of the inward currents showing no detectable Na^+ conductance by *Hv*MLO in HEK293T cells. Error bars depict means ± S.E.M. n values = 8 cells. All *P* values were determined by two-tailed Student's *t*-test.

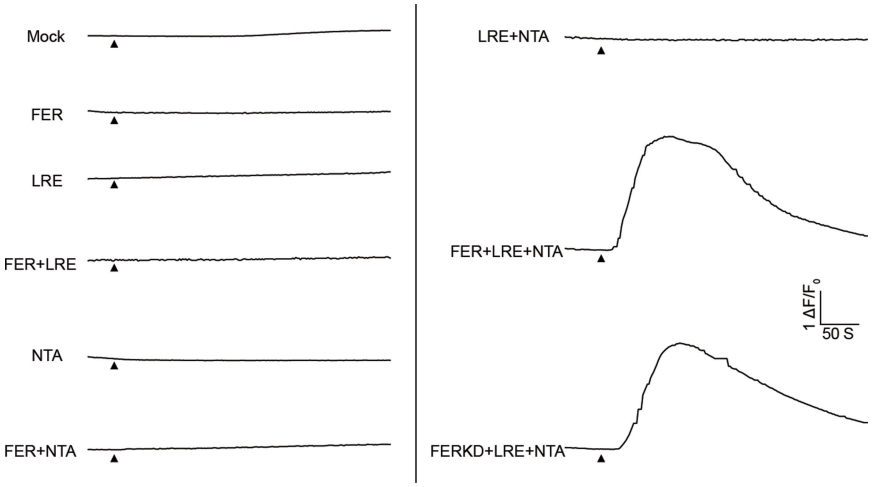

Extended Data Fig. 7 | Typical cytosolic Ca^{2+} increase curves of COS7 cells expressing the combination of FER, LRE, NTA and the kinase-dead version of FER (FERKD). The black triangle indicated the time point when 10 mM external Ca^{2+} was applied.

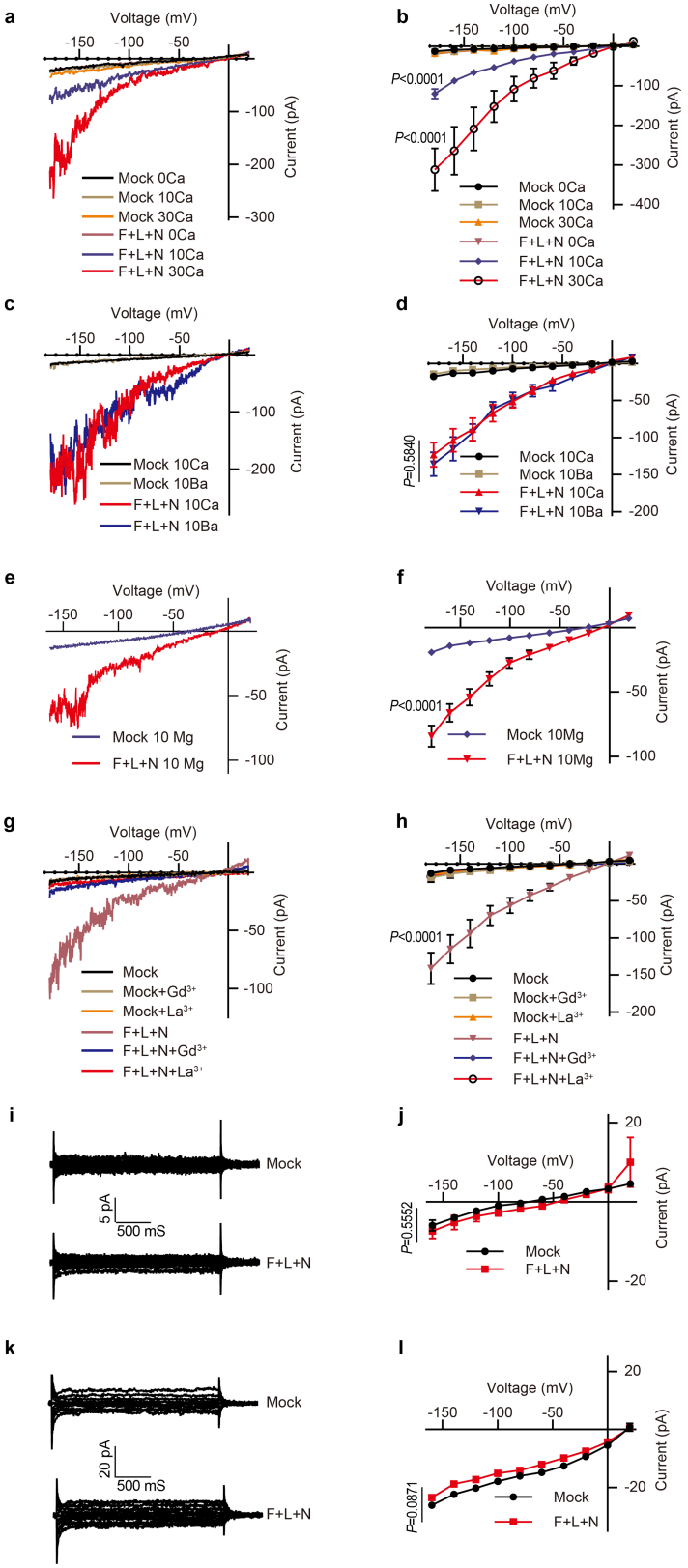

Extended Data Fig. 8 | Conductivity of NTA trio to divalent and monovalent cations. (**a**) Typical whole-cell recordings and (**b**) average current-voltage curves of the inward currents showing external Ca^{2+} dependence (0 mM, 10 mM and 30mM) in HEK293T cells expressing NTA trio. (**c**) Typical whole-cell recordings and (**d**) average current-voltage curves for Ba^{2+} conductance by NTA trio in HEK293T cells. (**e**) Typical whole-cell recordings and (**f**) average current-voltage curves for Mg^{2+} conductance by NTA trio in HEK293T cells. (**g**) Typical whole-cell recordings and (**h**) average current-voltage curves for Gd^{3+} (100 μM) and La^{3+} (100 μM) inhibition of Ca^{2+} conductance in HEK293T cells expressing NTA trio. (**i**) Typical whole-cell recordings and (**j**) average current-voltage curves of the inward currents showing no detectable K^+ conductance by NTA trio in HEK293T cells. (**k**) Typical whole-cell recordings and (**l**) average current-voltage curves of the inward currents showing no detectable Na^+ conductance by NTA trio in HEK293T cells. Error bars depict means ± S.E.M. n values = 8 cells. All *P* values were determined by two-tailed Student's *t*-test.

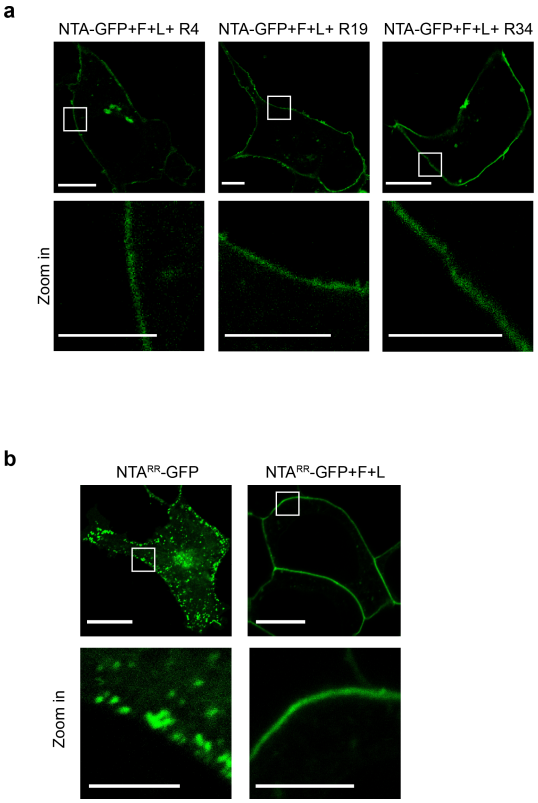

Extended Data Fig. 9 | The localization of NTA-GFP and NTA^{RR}-GFP. a, RALFs did not alter the PM localization of NTA-GFP. n = 3 independent repeats. **b**, FER and LRE facilitated the PM localization of NTA^{RR}-GFP. Scale bars, 10 μm (up-panel), 5 μm (down-panel). The white rectangle indicated the area of zoom-in. n = 3 independent repeats.

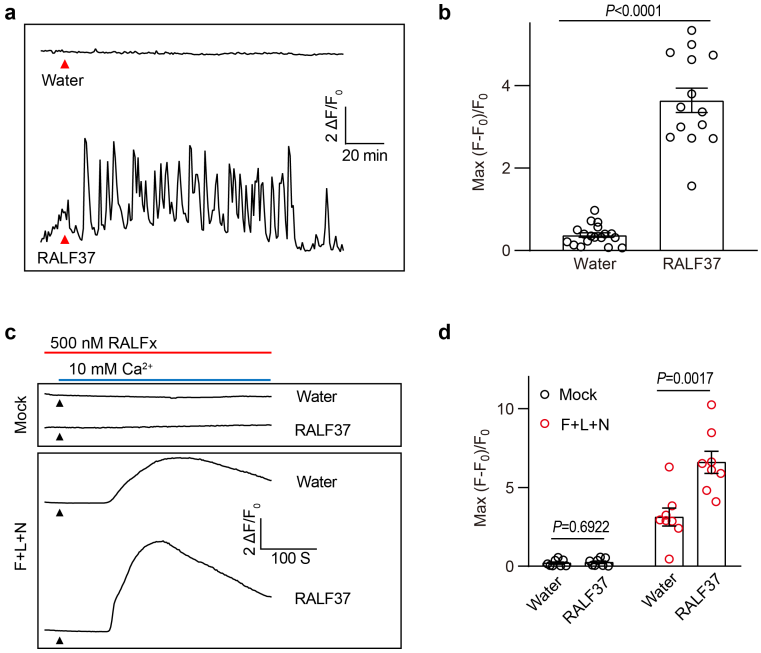

Extended Data Fig. 10 | RALF37 triggers synergid Ca^{2+} changes and enhances the activity of NTA trio. a, Representative Ca^{2+} spiking patterns in synergid cells in response to 0.5 µM RALF37. **b**, The peak values of Ca^{2+} spiking as in (**a**). n = 18 ovules for water treatment and n = 14 ovules for RALF37. **c**, **d**, Representative cytosolic Ca^{2+} spiking curves (**c**) and statistical analysis of peak values (**d**) in COS7 cells expressing the FER-LRE-NTA trio treated with 0.5 µM RALF37. n = 8 replicates, and ~ 60 cells were imaged in each duplicate. Error bars depict means ± S.E.M. All *P* values were determined by two-tailed Student's *t*-test.

nature portfolio

Corresponding author(s): Sheng Luan

Last updated by author(s): May 17, 2022

Reporting Summary

Nature Portfolio wishes to improve the reproducibility of the work that we publish. This form provides structure for consistency and transparency in reporting. For further information on Nature Portfolio policies, see our Editorial Policies and the Editorial Policy Checklist.

Statistics

For all statistical analyses, confirm that the following items are present in the figure legend, table legend, main text, or Methods section.

n/a	Confirmed	
☐	☒	The exact sample size (*n*) for each experimental group/condition, given as a discrete number and unit of measurement
☐	☒	A statement on whether measurements were taken from distinct samples or whether the same sample was measured repeatedly
☐	☒	The statistical test(s) used AND whether they are one- or two-sided *Only common tests should be described solely by name; describe more complex techniques in the Methods section.*
☐	☐	A description of all covariates tested
☐	☒	A description of any assumptions or corrections, such as tests of normality and adjustment for multiple comparisons
☐	☒	A full description of the statistical parameters including central tendency (e.g. means) or other basic estimates (e.g. regression coefficient) AND variation (e.g. standard deviation) or associated estimates of uncertainty (e.g. confidence intervals)
☐	☒	For null hypothesis testing, the test statistic (e.g. *F*, *t*, *r*) with confidence intervals, effect sizes, degrees of freedom and *P* value noted *Give P values as exact values whenever suitable.*
☐	☐	For Bayesian analysis, information on the choice of priors and Markov chain Monte Carlo settings
☐	☐	For hierarchical and complex designs, identification of the appropriate level for tests and full reporting of outcomes
☐	☐	Estimates of effect sizes (e.g. Cohen's *d*, Pearson's *r*), indicating how they were calculated

Our web collection on statistics for biologists contains articles on many of the points above.

Software and code

Policy information about availability of computer code

Data collection	ZEN 2012 was used to collect fluorescence signals from the co-focal microscopy; Clampex 10.7 was used for data acquisition in the patch-clamp experiments; Ivision4.5 (BioVision Technologies) was used for calcium imaging data acquisition.
Data analysis	Microsoft Excel in office 365 and GraphPad Prism 7.0 were used for calculation and statistical analysis of the data; Adobe Illustrator CC 2019 was used for image assembly; Clampfit 10.7 was used for data analysis and processing in electrophysiological experiments; Image J (1.51j8 version) was used to analyze calcium imaging data.

For manuscripts utilizing custom algorithms or software that are central to the research but not yet described in published literature, software must be made available to editors and reviewers. We strongly encourage code deposition in a community repository (e.g. GitHub). See the Nature Portfolio guidelines for submitting code & software for further information.

Data

Policy information about availability of data

All manuscripts must include a data availability statement. This statement should provide the following information, where applicable:

- Accession codes, unique identifiers, or web links for publicly available datasets
- A description of any restrictions on data availability
- For clinical datasets or third party data, please ensure that the statement adheres to our policy

The data supporting the findings of this study are available within the paper and its Supplementary Information files. Source Data for Figs. 1–4 and Extended Data Figs. 1–10 are provided with the paper.

Field-specific reporting

Please select the one below that is the best fit for your research. If you are not sure, read the appropriate sections before making your selection.

☒ Life sciences ☐ Behavioural & social sciences ☐ Ecological, evolutionary & environmental sciences

For a reference copy of the document with all sections, see nature.com/documents/nr-reporting-summary-flat.pdf

Life sciences study design

All studies must disclose on these points even when the disclosure is negative.

Sample size	No statistical methods were used to predetermine sample sizes. The exact number of samples in each experiment was specified in the figure legends. In all cases, sample sizes were adequate as the results were reproducible between different experimental groups. The sample size is chosen based on the pre-established criteria in the field, and they are sufficient to find the difference in our study.
Data exclusions	For TEVC experiments, damaged oocytes were discarded and not used for recording. Damaged oocyte produces leaky currents which interfere the conclusions. The exclusion criteria were pre-established in the field.
Replication	All attempts to replicate the experiments were successful. Each experiment was repeated for at least three times with similar results obtained. Number of repeats in each experiment was provided in the figure legends.
Randomization	Plants of different genotypes were randomly positioned in the growth chamber or in the greenhouse. For patch-clamp, the cells for recording were randomly selected. TEVC recording of Xenopus oocytes expressing different proteins were randomly performed. Randomization was not applied to western blot, because it is not relevant to it. In western blot, protein samples were loaded into the SDS-PAGE gel and transferred to the PVDF membrane evenly via electrical application. The solution evenly covered the membranes during antibody binding as a result of constant agitation of the solution in the bag, and then the western blotting luminol reagent were evenly added to the PVDF membrane for the chemiluminescence detection.
Blinding	Blinding was impossible in the experiments because the author who conducted the experiments also performed data acquisition and analysis.

Reporting for specific materials, systems and methods

We require information from authors about some types of materials, experimental systems and methods used in many studies. Here, indicate whether each material, system or method listed is relevant to your study. If you are not sure if a list item applies to your research, read the appropriate section before selecting a response.

Materials & experimental systems

n/a	Involved in the study
☐	☒ Antibodies
☐	☒ Eukaryotic cell lines
☐	☐ Palaeontology and archaeology
☐	☐ Animals and other organisms
☐	☐ Human research participants
☐	☐ Clinical data
☐	☐ Dual use research of concern

Methods

n/a	Involved in the study
☐	☐ ChIP-seq
☐	☐ Flow cytometry
☐	☐ MRI-based neuroimaging

Antibodies

Antibodies used	All antibodies except Anti-Flag are provided by Santa Cruz Biotechnology. (1) Anti-GST(B-14): sc-138HRP,Lot:A2513(1: 2 000 dilution); (2) Anti-cMyc Antibody (9E10): sc-40HRP,Lot:L1520(1: 2 000 dilution); (3) Anti-MBP-probe Antibody (R29.6): sc-13564,Lot:A2921(1: 2 000 dilution); (4)Anti-HA-Tag Antibody (F-7): sc-7392,Lot:E1818(1: 2 000 dilution); (5)Anti-mouse Secondary antibody:m-IgGk BP-HRP: sc-516102, Lot:J1320(1:20 000 dilution) . Anti-Flag is provided by Sigma-Aldrich Chemicals company: A8592-1MG, Lot:SLCF0816(1: 4 000 dilution) .
Validation	These antibodies have been validated by the manufacture. (1) Anti-GST https://www.scbt.com/p/gst-antibody-b-14; (2)Anti-cMyc https://www.scbt.com/p/c-myc-antibody-9e10; (3)Anti-MBP https://www.scbt.com/p/mbp-probe-antibody-r29-6; (4)Anti-HA https://www.scbt.com/p/ha-probe-antibody-f-7; (5) Anti-Flag https://www.sigmaaldrich.com/US/en/product/sigma/a8592

Eukaryotic cell lines

Policy information about cell lines

Cell line source(s)	HEK293T(Human embryonic kidney 293T) cell , COS7 (Monkey Kidney cell) cell and High5 (BTI-Tn-5B1-4) cells are all from ATCC (https://www.atcc.org/)
Authentication	The cells have been authenticated by Short Tandem Repeat (STR) DNA profiling
Mycoplasma contamination	The three cell lines are negative for Mycoplasma contamination
Commonly misidentified lines (See ICLAC register)	None of the cell lines used are listed in the ICLAC database.

Palaeontology and Archaeology

Specimen provenance	*Provide provenance information for specimens and describe permits that were obtained for the work (including the name of the issuing authority, the date of issue, and any identifying information). Permits should encompass collection and, where applicable, export.*
Specimen deposition	*Indicate where the specimens have been deposited to permit free access by other researchers.*
Dating methods	*If new dates are provided, describe how they were obtained (e.g. collection, storage, sample pretreatment and measurement), where they were obtained (i.e. lab name), the calibration program and the protocol for quality assurance OR state that no new dates are provided.*

☐ Tick this box to confirm that the raw and calibrated dates are available in the paper or in Supplementary Information.

Ethics oversight	*Identify the organization(s) that approved or provided guidance on the study protocol, OR state that no ethical approval or guidance was required and explain why not.*

Note that full information on the approval of the study protocol must also be provided in the manuscript.

Animals and other organisms

Policy information about studies involving animals; ARRIVE guidelines recommended for reporting animal research

Laboratory animals	*For laboratory animals, report species, strain, sex and age OR state that the study did not involve laboratory animals.*
Wild animals	*Provide details on animals observed in or captured in the field; report species, sex and age where possible. Describe how animals were caught and transported and what happened to captive animals after the study (if killed, explain why and describe method; if released, say where and when) OR state that the study did not involve wild animals.*
Field-collected samples	*For laboratory work with field-collected samples, describe all relevant parameters such as housing, maintenance, temperature, photoperiod and end-of-experiment protocol OR state that the study did not involve samples collected from the field.*
Ethics oversight	*Identify the organization(s) that approved or provided guidance on the study protocol, OR state that no ethical approval or guidance was required and explain why not.*

Note that full information on the approval of the study protocol must also be provided in the manuscript.

Human research participants

Policy information about studies involving human research participants

Population characteristics	*Describe the covariate-relevant population characteristics of the human research participants (e.g. age, gender, genotypic information, past and current diagnosis and treatment categories). If you filled out the behavioural & social sciences study design questions and have nothing to add here, write "See above."*
Recruitment	*Describe how participants were recruited. Outline any potential self-selection bias or other biases that may be present and how these are likely to impact results.*
Ethics oversight	*Identify the organization(s) that approved the study protocol.*

Note that full information on the approval of the study protocol must also be provided in the manuscript.

Clinical data

Policy information about clinical studies

All manuscripts should comply with the ICMJE guidelines for publication of clinical research and a completed CONSORT checklist must be included with all submissions.

Clinical trial registration	*Provide the trial registration number from ClinicalTrials.gov or an equivalent agency.*

Study protocol	*Note where the full trial protocol can be accessed OR if not available, explain why.*
Data collection	*Describe the settings and locales of data collection, noting the time periods of recruitment and data collection.*
Outcomes	*Describe how you pre-defined primary and secondary outcome measures and how you assessed these measures.*

Dual use research of concern

Policy information about dual use research of concern

Hazards

Could the accidental, deliberate or reckless misuse of agents or technologies generated in the work, or the application of information presented in the manuscript, pose a threat to:

No	Yes	
☐	☐	Public health
☐	☐	National security
☐	☐	Crops and/or livestock
☐	☐	Ecosystems
☐	☐	Any other significant area

Experiments of concern

Does the work involve any of these experiments of concern:

No	Yes	
☐	☐	Demonstrate how to render a vaccine ineffective
☐	☐	Confer resistance to therapeutically useful antibiotics or antiviral agents
☐	☐	Enhance the virulence of a pathogen or render a nonpathogen virulent
☐	☐	Increase transmissibility of a pathogen
☐	☐	Alter the host range of a pathogen
☐	☐	Enable evasion of diagnostic/detection modalities
☐	☐	Enable the weaponization of a biological agent or toxin
☐	☐	Any other potentially harmful combination of experiments and agents

ChIP-seq

Data deposition

☐ Confirm that both raw and final processed data have been deposited in a public database such as GEO.

☐ Confirm that you have deposited or provided access to graph files (e.g. BED files) for the called peaks.

Data access links *May remain private before publication.*	*For "Initial submission" or "Revised version" documents, provide reviewer access links. For your "Final submission" document, provide a link to the deposited data.*
Files in database submission	*Provide a list of all files available in the database submission.*
Genome browser session (e.g. UCSC)	*Provide a link to an anonymized genome browser session for "Initial submission" and "Revised version" documents only, to enable peer review. Write "no longer applicable" for "Final submission" documents.*

Methodology

Replicates	*Describe the experimental replicates, specifying number, type and replicate agreement.*
Sequencing depth	*Describe the sequencing depth for each experiment, providing the total number of reads, uniquely mapped reads, length of reads and whether they were paired- or single-end.*
Antibodies	*Describe the antibodies used for the ChIP-seq experiments; as applicable, provide supplier name, catalog number, clone name, and lot number.*
Peak calling parameters	*Specify the command line program and parameters used for read mapping and peak calling, including the ChIP, control and index files used.*

Data quality	*Describe the methods used to ensure data quality in full detail, including how many peaks are at FDR 5% and above 5-fold enrichment.*
Software	*Describe the software used to collect and analyze the ChIP-seq data. For custom code that has been deposited into a community repository, provide accession details.*

Flow Cytometry

Plots

Confirm that:

☐ The axis labels state the marker and fluorochrome used (e.g. CD4-FITC).

☐ The axis scales are clearly visible. Include numbers along axes only for bottom left plot of group (a 'group' is an analysis of identical markers).

☐ All plots are contour plots with outliers or pseudocolor plots.

☐ A numerical value for number of cells or percentage (with statistics) is provided.

Methodology

Sample preparation	*Describe the sample preparation, detailing the biological source of the cells and any tissue processing steps used.*
Instrument	*Identify the instrument used for data collection, specifying make and model number.*
Software	*Describe the software used to collect and analyze the flow cytometry data. For custom code that has been deposited into a community repository, provide accession details.*
Cell population abundance	*Describe the abundance of the relevant cell populations within post-sort fractions, providing details on the purity of the samples and how it was determined.*
Gating strategy	*Describe the gating strategy used for all relevant experiments, specifying the preliminary FSC/SSC gates of the starting cell population, indicating where boundaries between "positive" and "negative" staining cell populations are defined.*

☐ Tick this box to confirm that a figure exemplifying the gating strategy is provided in the Supplementary Information.

Magnetic resonance imaging

Experimental design

Design type	*Indicate task or resting state; event-related or block design.*
Design specifications	*Specify the number of blocks, trials or experimental units per session and/or subject, and specify the length of each trial or block (if trials are blocked) and interval between trials.*
Behavioral performance measures	*State number and/or type of variables recorded (e.g. correct button press, response time) and what statistics were used to establish that the subjects were performing the task as expected (e.g. mean, range, and/or standard deviation across subjects).*

Acquisition

Imaging type(s)	*Specify: functional, structural, diffusion, perfusion.*
Field strength	*Specify in Tesla*
Sequence & imaging parameters	*Specify the pulse sequence type (gradient echo, spin echo, etc.), imaging type (EPI, spiral, etc.), field of view, matrix size, slice thickness, orientation and TE/TR/flip angle.*
Area of acquisition	*State whether a whole brain scan was used OR define the area of acquisition, describing how the region was determined.*

Diffusion MRI ☐ Used ☐ Not used

Preprocessing

Preprocessing software	*Provide detail on software version and revision number and on specific parameters (model/functions, brain extraction, segmentation, smoothing kernel size, etc.).*
Normalization	*If data were normalized/standardized, describe the approach(es): specify linear or non-linear and define image types used for transformation OR indicate that data were not normalized and explain rationale for lack of normalization.*
Normalization template	*Describe the template used for normalization/transformation, specifying subject space or group standardized space (e.g.*

Normalization template

original Talairach, MNI305, ICBM152) OR indicate that the data were not normalized.

Noise and artifact removal

Describe your procedure(s) for artifact and structured noise removal, specifying motion parameters, tissue signals and physiological signals (heart rate, respiration).

Volume censoring

Define your software and/or method and criteria for volume censoring, and state the extent of such censoring.

Statistical modeling & inference

Model type and settings

Specify type (mass univariate, multivariate, RSA, predictive, etc.) and describe essential details of the model at the first and second levels (e.g. fixed, random or mixed effects; drift or auto-correlation).

Effect(s) tested

Define precise effect in terms of the task or stimulus conditions instead of psychological concepts and indicate whether ANOVA or factorial designs were used.

Specify type of analysis: ☐ Whole brain ☐ ROI-based ☐ Both

Statistic type for inference
(See Eklund et al. 2016)

Specify voxel-wise or cluster-wise and report all relevant parameters for cluster-wise methods.

Correction

Describe the type of correction and how it is obtained for multiple comparisons (e.g. FWE, FDR, permutation or Monte Carlo).

Models & analysis

n/a	Involved in the study
☐	☐ Functional and/or effective connectivity
☐	☐ Graph analysis
☐	☐ Multivariate modeling or predictive analysis

Functional and/or effective connectivity

Report the measures of dependence used and the model details (e.g. Pearson correlation, partial correlation, mutual information).

Graph analysis

Report the dependent variable and connectivity measure, specifying weighted graph or binarized graph, subject- or group-level, and the global and/or node summaries used (e.g. clustering coefficient, efficiency, etc.).

Multivariate modeling and predictive analysis

Specify independent variables, features extraction and dimension reduction, model, training and evaluation metrics.